



HAL
open science

A subset of flavaglines inhibits KRAS nanoclustering and activation

Hajime Yurugi, Yinyin Zhuang, Farid A Siddiqui, Hong Liang, Sebastian Rosigkeit, Yongpeng Zeng, Hussein Abou-Hamdan, Ernesto Bockamp, Yong Zhou, Daniel Abankwa, et al.

► To cite this version:

Hajime Yurugi, Yinyin Zhuang, Farid A Siddiqui, Hong Liang, Sebastian Rosigkeit, et al.. A subset of flavaglines inhibits KRAS nanoclustering and activation. *Journal of Cell Science*, 2020, 133 (12), pp.jcs244111. 10.1242/jcs.244111 . hal-02996708

HAL Id: hal-02996708

<https://hal.science/hal-02996708>

Submitted on 9 Nov 2020

HAL is a multi-disciplinary open access archive for the deposit and dissemination of scientific research documents, whether they are published or not. The documents may come from teaching and research institutions in France or abroad, or from public or private research centers.

L'archive ouverte pluridisciplinaire **HAL**, est destinée au dépôt et à la diffusion de documents scientifiques de niveau recherche, publiés ou non, émanant des établissements d'enseignement et de recherche français ou étrangers, des laboratoires publics ou privés.

A subset of flavaglines inhibits KRAS nanoclustering and activation

Hajime Yurugi¹, Yinyin Zhuang², Farid A Siddiqui³, Hong Liang⁴, Sebastian Rosigkeit¹, Yongpeng Zeng², Hussein Abou-Hamdan⁵, Ernesto Bockamp⁶, Yong Zhou⁴, Daniel Abankwa^{3,7}, Wenting Zhao², Laurent Désaubry⁵, Krishnaraj Rajalingam^{1,8}

¹ Cell Biology Unit, University Medical Center Mainz, Johannes Gutenberg University - Mainz, Germany

² School of Chemical and Biomedical Engineering, Nanyang Technological University Singapore

³ Turku Centre for Biotechnology, Åbo Akademi University, Tykistökatu 6B, 20520 Turku, Finland,

⁴ Department of Integrative Biology and Pharmacology, McGovern Medical School, UT Health, 6431 Fannin St. MSE R382, Houston, Texas 77030

⁵ Therapeutic Laboratory of Cardio-Oncology and Medicinal Chemistry (FRE 2033), CNRS, University of Strasbourg, 4 rue Blaise Pascal, CS 90032, 67081 Strasbourg, France

⁶ Institute for Translational Immunology and Research Center for Immunotherapy, University Medical Center, Johannes Gutenberg University, D 55131 Mainz, Germany

.

⁷ Cancer Cell Biology and Drug Discovery Group, Life Sciences Research Unit University of Luxembourg, Esch-sur-Alzette, Luxembourg

⁸ University Cancer Center Mainz, University Medical Center Mainz, Mainz, Germany

Address for Correspondence: *Krishna@uni-mainz.de*

The authors declare that they have no conflict of interest

Abstract

RAS oncogenes are frequently mutated in human cancers and among the three isoforms (KRAS, HRAS and NRAS), KRAS is the most frequently mutated oncogene. Here we demonstrate that a subset of flavaglines, a class of natural anti-tumour drugs and chemical ligands of prohibitins, inhibit RAS GTP loading and oncogene activation in cells at nanomolar concentrations. Treatment with rocaglamide, the first discovered flavagline, inhibited the nanoclustering of KRAS, but not HRAS and NRAS, at specific phospholipid enriched plasma membrane domains. We further demonstrate that plasma membrane-associated prohibitins directly interact with KRAS, phosphatidyl serine and phosphatidic acid, and these interactions are disrupted by rocaglamide but not by a structurally related flavagline **FL1**. Depletion of prohibitin-1 phenocopied rocaglamide-mediated effects on RAS activation and stability. We also demonstrate that flavaglines inhibit the oncogenic growth of KRAS-mutated cells and treatment with rocaglamide reduces NSCLC tumours in autochthonous KRAS-driven mouse models without severe side effects. Our data suggest that it will be promising to further develop flavagline derivatives as specific KRAS inhibitors for clinical applications.

Introduction

RAS proteins are small GTPases that function as molecular switches regulating the transmission of extracellular signals from the outside of the cell to the nucleus by various effector proteins (Hobbs et al., 2016; Ostrem and Shokat, 2016; Simanshu et al., 2017). Their activation cycle is regulated by the binding of GDP or GTP, which in turn is controlled by GAPs or GEFs. In their GTP-bound form RAS proteins bind to several effectors and trigger multiple signalling pathways that control various fundamental cellular processes. The most common mutations in codons 12, 13 and 61 prevent GAP mediated GTP hydrolysis of RAS thus keeping it constitutively in the GTP-bound, active state. Through alternative splicing, two KRAS isoforms are generated (KRAS4A and KRAS4B), though KRAS4B is predominantly expressed in most cancers (Tsai et al., 2015). Most of the mutations in RAS isoforms are confined to three hotspot residues (G12, G13 and Q61) whose mutations lead to distinct biological consequences (COSMIC) (Ihle et al., 2012).

Recently drugs directly targeting specifically the KRAS G12C mutant have entered clinical trials (Khan et al., 2020; Ostrem and Shokat, 2016). The three RAS isoforms exhibit 82-90% sequence identity and most of the differences are confined to the C-terminal HVR region. While KRAS mutations are frequently identified in pancreatic, lung and colon carcinomas, NRAS mutations predominate in melanomas and HRAS mutations in head and neck cancers. The molecular consequences caused by the isoform-specific RAS mutations and their tissue-specific roles are currently unclear. There are also significant differences between the RAS isoforms with respect to their posttranslational modifications and their intracellular localization. KRAS4A and KRAS4B have polybasic stretches that are responsible for their affinity to phospholipids in lipid nanoclusters of the plasma membrane (Zhou and Hancock, 2015). KRAS4B can also be phosphorylated at S181 which might dictate its localization to endomembranes. While HRAS is palmitoylated at two residues, KRAS4A and NRAS are palmitoylated at a single residue in the HVR region. These modifications determine their distribution within the plasma membrane microdomains which in turn dictates the downstream signalling (Hancock and Parton, 2005).

Here, we show that targeting plasma membrane-associated prohibitins with a subset of flavaglines inhibits the GTP-loading of RAS, thereby leading to inactivation of this GTPase. Flavaglines are natural anti-tumour drugs isolated from plants of the genus

Aglaia characterized by a cyclopenta[*b*]benzofuran ring that directly targets prohibitins 1 and 2 and eukaryotic initiation factor-4A (eIF4A) (Chu et al., 2020; Ebada et al., 2011; Ribeiro et al., 2012). PHB1 and PHB2 are evolutionarily conserved proteins predominantly known for their roles in the regulation mitochondrial function and cristae morphogenesis (Merkwirth and Langer, 2009; Mishra et al., 2010). Prohibitins are members of the SPFH family of membrane proteins with PHB domains (Browman et al., 2007). They are often detected in distinct subdomains of the plasma membrane, and they form functional oligomers, which dictate the formation of a signalling and functional unit at the plasma membrane (Kim et al., 2013; Yurugi et al., 2012). Previous studies have shown that PHB1 directly binds to CRAF kinase and is required for its activation (Rajalingam et al., 2005). Several biological and chemical ligands of prohibitins that target the prohibitin complex (PHB1 and PHB2) at the plasma membrane have been identified (Thuaud et al., 2013). Two PHB ligands, fluorizoline and rocaglamide, inhibit the interaction between PHB1 and CRAF and inhibit KRAS-mediated tumorigenesis (Yurugi et al., 2017). However, activated BRAF(V600E), which can directly phosphorylate MEK1/2 and activate the MAPK pathway, overcomes the anti-tumor effects of fluorizoline and rocaglamide (Yurugi et al., 2017). Here, we investigated the underlying mechanisms of flavagline action and show that only a subset of flavaglines with defined side chains inhibit RAS activation in cells. We identify that rocaglamide prevented the interaction between prohibitins, KRAS, and specific phospholipids in the plasma membrane. Furthermore, rocaglamide inhibits the growth of KRAS-driven tumors in autochthonous mouse models.

Results

We have previously shown that treatment with rocaglamide inhibits RAS-GTP loading in cells upon EGF stimulation (Yurugi et al., 2017). In all these experiments we primarily employed CRAF-RBD domain for precipitating active GTP-bound RAS. To rule out the possibility that rocaglamide inhibits primarily the interaction between KRAS and the Ras-binding domain (RBD) of CRAF, we detected GTP-loaded RAS upon pull down with CRAF-RBD and Ral-GDS-RA domains. Activation of RAS in response to EGF was inhibited upon pre-treatment of HeLa cells with rocaglamide at 200 nM concentration (Fig. S1A). In these early time points post treatment, we could not detect any significant changes in Cyclin D1 a known

substrate of eIF4F complex (Fig. S1A). Further, these results also suggest that the inhibition is not dependent on the RAS binding domain employed in the assay. Despite the extremely high affinity of abundant GTP to RAS in cells, rocaglamide treatment inhibited this interaction in cells.

Next, we established a NanoBiT assay (live cell Nano-luciferase complementation assay) (Oh-Hashi et al., 2016) with KRAS and CRAF-RBD to quantify activation of KRAS (Fig. 1A). We validated the sensitivity of this NanoBiT assay with wild-type, active, and inactive mutants of KRAS that confirms the GTP driven binding between KRAS and CRAF-RBD (Fig. S1B). We then tested the effect of rocaglamide on gain-of-function KRAS mutants. Rocaglamide strongly reduced the interaction between each of the KRAS mutants and CRAF-RBD (Fig. 1B, Fig. S1C, S1D). These data and those from the RBD pull-down experiment (Fig. S1A) suggested that rocaglamide inhibits KRAS activation and thus the effector binding in cells.

Compared to the RBD pull-down assay, the NanoBit assay is quantitative and can be used to calculate affinity and kinetic parameters. We determined with the NanoBit assay that rocaglamide inhibits KRAS activation with an IC₅₀ of 24.8 nM (Fig. 1C), and that 100 nM of rocaglamide produced 50% inhibition by 50 minutes (Fig. 1D, Fig. S1E). The results also show that rocaglamide inhibits KRAS4A activated either by EGF stimulation or by gain of function mutations (Fig. S1F and G). Recent studies led to the successful development of a KRAS G12C inhibitor which entered clinical trial (<https://clinicaltrials.gov/ct2/show/NCT03600883>). For further validation of our NanoBiT assay, we included KRAS G12C inhibitor (ARS-1620) in our experiments (Janes et al., 2018). As shown in Fig. 1E, ARS-1620 strongly inhibited KRAS G12C mutants while the G12V mutant was only modestly inhibited by the treatment. In contrast, treatment with rocaglamide inhibited both KRAS mutants to the same extent (Fig. 1F). This data confirms that rocaglamide is not biased towards specific KRAS mutants, which is valuable as recent studies called for combined inhibition of both wild type and mutant KRAS due to feedback reactivation of wildtype RAS through activation of Receptor Tyrosine Kinases in a panel of *KRAS*^{G12C} cell lines treated with ARS-1620 and AMG 510 (Ryan et al., 2019). We then tested whether rocaglamide treatment can inhibit other RAS isoforms by NanoBit assays and found that rocaglamide but not a closely related flavagline FL1 inhibited all the three RAS isoforms (Fig. 1G).

To further evaluate the inhibition of KRAS with other flavaglines, we selectively employed 17 different flavaglines, which differ in their side chains (Fig. S2). Using NanoBiT assays we detected that apart from rocaglamide only a subset of flavaglines was able to inhibit KRAS (FL3, FL10, FL13, FL15, FL19, FL23, FL32, FL37, FL40, FL42). While the degree of inhibition slightly varied among the different flavaglines, some members (like FL1, FL6, FL26 and FL30) failed completely to inhibit KRAS activation, indicating that the substituents on the cyclopenta[*b*]benzofuran skeleton are critical for the ability to inhibit KRAS (Fig. 2A and 2B). As we expected, the pattern of KRAS inhibition aligned with the inhibition of the downstream MAP2K MEK1/2 (Fig. 2C and 2D). More precisely, the suppression of the methoxy in position 8 was highly detrimental, while the hydroxyl in position 1 could be replaced by a formamide or dimethylurea with the opposite configuration. The introduction of a dimethylcarboxamide, methylcarboxamide or methyl ester promoted the anti-KRAS activity. The introduction of a fluorine in position 3' enhanced or lowered the anti-KRAS activity depending upon the other substituents in position 1' and 4'. The replacement of the methoxy in position 4' by a bromine or a chlorine promoted the anti-KRAS activity (Fig. 2E). We performed validation experiments with specific flavaglines for the inhibition of different KRAS mutations and RAS isoforms. As expected, apart from rocaglamide, FL3, FL10, FL23 and FL42 but not FL1 and FL6 inhibited activation of KRAS and other RAS isoforms (Fig 2F-H).

Because rocaglamide inhibits the interaction between CRAF and PHB1 (Polier et al., 2012; Yurugi et al., 2017) we tested whether the inhibition of RAS activation was dependent on CRAF. As expected, depletion of CRAF failed to prevent EGF-mediated RAS activation, suggesting that inhibition of CRAF is not influencing RAS activation under these settings (Fig. S3A). Further rocaglamide treatment failed to prevent the activating phosphorylation of EGFR in response to EGF stimulation suggesting that the effects observed are downstream of EGFR activation (Fig. S3B). We then tested whether rocaglamide treatment inflicts structural changes to RAS in cells. Indeed, addition of GTP γ S to RAS precipitated from rocaglamide-treated cells rescued GTP-loading (Fig. S3C, Fig. S3D), indicating that rocaglamide treatment did not cause irreversible structural and/or functional modifications to RAS.

We then tested whether treatment with selected flavaglines (rocaglamide and FL42) inhibits the growth of cancer cells *in vitro* by employing soft agar colony formation assays. Apart from rocaglamide we have selected FL42 for subsequent experiments as

FL42 has been previously shown to have no effect on eIF4A function, the other proposed target of rocaglamide (Boussemart et al., 2014). In MTT assays, both flavaglines were very effective in blocking the growth of HCT-116, ASPC-1, and Calu-1 cells, which carry KRAS mutations with an IC50 in the low nanomolar range (6-20 nM, Fig. 3A). The treatment also inhibited growth of HCT-116 and ASPC-1 cells in soft agar (Fig. 3B and 3C). We then expanded the panel of flavaglines in soft agar colony forming assays including ones that failed to inhibit KRAS activation. These results were consistent with the results obtained with RAS inhibition (Fig. 2F-H, Fig. 3D). Together, these data suggest that a subset of flavaglines can inhibit KRAS activation and prevent the oncogenic growth of tumour cells *in vitro* though the latter effect could also be attributed to the additive inhibition of eIF4F complex.

To test the effects of rocaglamide *in vivo*, we employed an autochthonous KRAS G12D-driven NSCLC mouse model as detailed in the methods section. The expression of KRAS G12D was induced with doxycycline treatment for 2 months followed by treatment of the mice with rocaglamide at a concentration of 2.5 mg/kg i.p. 3 times a week for 6 weeks. Rocaglamide treatment reduced the number of lung nodules suggesting a successful inhibition of the growth and maintenance of KRAS G12D-driven NSCLC model (Fig. 3D, Fig. S4). To address potential toxic effects of long-term rocaglamide treatment, we also tested liver and kidney toxicity in two different mouse strains. We did not detect any toxic effects as measured by liver enzyme activities and the blood creatine levels in two different mouse strains at the concentrations employed (Fig. S5). As rocaglamide also inhibits eIF4A, we tested the effect of rocaglamide in influencing the growth of BRAF-mutated cell lines as the MAPK pathway is constitutively activated. As expected, the growth of BRAF mutated cells was also inhibited by rocaglamide treatment though with varying efficiency (Fig. S6). These data suggested that the long term phenotypic effects on cell growth by rocaglamide could possibly attributed to the inhibition of both RAS and eIF4F complex though further experiments are clearly warranted with other flavaglines that do not inhibit eIF4A like FL42.

We then explored the molecular mechanisms behind rocaglamide-mediated inhibition of KRAS activation in cells. Nanoclustering of KRAS is required for the activation of downstream effectors like the RAF kinases (Abankwa et al., 2010; Zhou and Hancock, 2015). Using FLIM-FRET imaging of RAS-isoform FRET-pairs (Solman et al., 2015), we detected that treatment with nanomolar concentrations of rocaglamide

prevents KRAS nanoclustering-associated FRET but not FRET indicative of HRAS or NRAS nanoclusters (Fig. 4A-C). Consistent with these studies, immunogold labelling coupled to electron microscopic analysis of RAS proteins revealed that rocaglamide inhibited nanoclustering of KRAS but not NRAS or HRAS (Fig. 4D-G). These results are intriguing because we detected rocaglamide-mediated inhibition of HRAS and NRAS in the NanoBiT assay, which measures primarily GTP-driven binding to its effector.

To study the dynamics of KRAS activation, we cultured cells onto nanobar substrates to generate patterns on plasma membrane and to measure curvature response. Consistent with a recent study (Liang et al., 2019) activated KRAS formed clusters preferentially at the end of the nanobars, unlike the wild type KRAS (Fig. 5A-C). Treatment with rocaglamide reversed the bar end preference (marked by bar end to center ratio) of activated KRAS on these nanobars phenocopying the KRAS wild type distribution pattern (Fig. 5D-G). Interestingly, PHB1 was also enriched at the end of the nanobars like KRAS (Fig. S7). Together with the FLIM-FRET and electron microscopic analyses, these data indicated that rocaglamide treatment inhibited the formation of KRAS clusters at the plasma membrane leading to KRAS inactivation.

Because PHB1 and KRAS showed a similar distribution pattern on nanobars, we tested the interaction between activated KRAS G12D and PHB1 by performing biochemical assays in cells with crosslinking agents. As expected, PHB1 coimmunoprecipitated with KRAS G12D protein and the interaction was increased after crosslinking (Fig. 6A). Thus, we performed a bimolecular fluorescence complementation assay (BiFC) (Fig. 6B) which confirmed the interaction between PHB1 and KRAS in living cells (Fig. 6C).

Finally, we performed a cellular thermal shift assay (CETSA) to test if PHBs serve as the direct targets of rocaglamide and active flavaglines like FL42. These experiments revealed that the PHB1-RAS complex is stabilized even at 50°C upon treatment with rocaglamide and FL42, but not with FL1 thus confirming the specificity of the observed effects (Fig. 6D). Under these settings we could not detect any significant changes to the levels of eIF4A (Fig. 6D). To further corroborate these observations we employed PHB1 siRNAs. As expected transient depletion of PHB1 in HeLa cells prevented RAS activation upon EGF stimulation as shown by Western blotting (Fig. 6E-F) and in a NanoBiT assay (Fig. 6G). These data suggested that the PHB1 is required for interaction of active RAS with CRAF kinase.

KRAS but not HRAS and NRAS nanoclustering is driven by phospholipids like phosphatidic acid (PA) and phosphatidyl serine (PS) (Ryan et al., 2019; Zhou et al., 2017). Previous studies have shown that prohibitins can function as phospholipid scaffolds in mitochondria such as cardiolipin (Osman et al., 2009). We confirmed that PHB1 precipitated from cells specifically binds to PS and PA, which can be reversed by rocaglamide (Fig. 7A). Using FLIM-FRET analysis we revealed that treatment with rocaglamide in fact inhibited clustering of KRAS with both PS and PA (Fig. 7B). These results indicate that rocaglamide specifically inhibits KRAS nanoclustering and effector protein activation possibly by influencing the prohibitin-dependent segregation of lipids within the plasma membrane.

Discussion

Treatment with a subset of flavaglines directly inhibited KRAS GTP-loading when cells were stimulated with EGF or when harbouring gain of function mutations at low nanomolar concentrations, thus functioning as potent KRAS inhibitor. Our results confirm that flavaglines inhibit KRAS but not HRAS and NRAS nanoclustering suggesting that PHB1-mediated segregation of phospholipids (PS and PA in specific) is probably required for maintaining the active KRAS conformation in cells. Though presence of membrane or lipids are not required for the GTP loading to KRAS, which is indeed a high affinity interaction in the picomolar range, flavagline treatment prevented KRAS GTP loading, which was reversed by exogenous addition of GTP γ S in solution. These effects are reproduced by the depletion of PHB1, which suggests a direct role for PHB1 in the regulation of KRAS activation.

Treatment with a subset of flavaglines also inhibited NRAS and HRAS activation as measured by the Nanobit assay though rocaglamide treatment failed to inhibit the nanoclustering of these two RAS isoforms. Previous studies have shown that NRAS and HRAS bind to different phospholipids other than KRAS for their nanoclustering (Ryan et al., 2019; Zhou et al., 2017). Further studies are clearly warranted to clarify this phenotype and the underlying mechanisms. KRAS is one of the most frequently mutated oncogene and several efforts are being made to target this oncogene in tumours. Our observations suggest treatment with rocaglamide disrupts the PHB-phospholipid-KRAS complex thus preventing effector protein activation (Fig. 8). Our study revealed a natural anti-tumour drug that potently inhibits KRAS at nanomolar concentrations irrespective of the mutations both *in vitro* cell culture models as well

as in autochthonous mouse models. These observations suggest that flavaglines should be further pursued for clinical development.

Materials and Methods

Cells

Calu-1 cells were obtained from Sigma-Aldrich and cultured in McCoy's 5A medium (10 % heat inactivated FBS). HeLa S3 (DSMZ), HEK-293T, and HCT-116 (a gift from Ulf Rapp) were authenticated by Eurofin genomics and these cells were cultured in DMEM (10 % heat inactivated FBS). ASPC-1 cells and NCI-H2122 cells were purchased from DSMZ and ATCC, respectively. These cells were cultured in RPMI-1640 (10 % heat inactivated FBS). HEK 293 EBNA (ATCC) and U-2OS cells (ATCC) were cultured in DMEM (10 % FBS). HeLa cells were starved in the serum free medium with rocaglamide or other flavaglines for various time points and stimulated with EGF (100 ng/ml) for 30 min. KRAS mutation carrying cells were treated with rocaglamide or FL1 in complete growth medium for 24 h.

Synthesis of flavaglines

Rocaglamide was a gift from Dr. Marcus Dobler (Syngenta, Basel Switzerland). Large scale synthesis was performed by Activ Biochem. The synthetic flavaglines were prepared as previously described (Ribeiro et al., 2012; Thuaud et al., 2009; Thuaud et al., 2011).

Active RAS-GTP pull down assay

After stimulation or treatment, active RAS pull-down buffer (25 mM Tris-HCl pH 7.2, 150 mM NaCl, 5 mM MgCl₂, 1% NP-40, 5% glycerol with protease inhibitor cocktail) was added to each well, and plates were incubated on ice for 30 min. Cells were sonicated for 3 sec and the lysate was centrifuged for 15 min at 4°C, 13000 rpm. Protein concentration was measured by 660 nm protein assay reagent (Thermo Scientific) and adjusted so that each sample had an equal concentration. Before the affinity pull down based RAS activation assay, 20% of the lysates was taken for the total cell lysate. CRAF-RBD-immobilised agarose beads (20 µl) were added to the rest of the lysate and rotated at 4°C for 60 min. After incubation, the beads were

washed with binding buffer twice, and 50 μ l of SDS-PAGE sample buffer (125 mM Tris-HCl pH 6.8, 4% SDS, 10% glycerol, BPB) were added.

SDS-PAGE and Western blotting

The samples were subjected to 14% SDS-PAGE followed by Western blotting. After transfer, the membrane was blocked with 3% BSA/TBST (20mM Tris-HCl, pH 7.5, 150mM NaCl, 0.05% Tween-20) for 1 h at room temperature. The membrane was incubated with primary antibody diluted in 1% BSA/TBST and incubated overnight at 4°C. After the overnight incubation, the membrane was washed with TBST (5 min x 5) and incubated with HRP-conjugated secondary antibody in TBST for 1 h at room temperature. After the secondary antibody treatment, the membrane was washed and the signal was visualized by chemiluminescence substrate (Millipore) and Chemi Doc touch (Bio-Rad). A list of antibodies is provided in supplementary table 1.

NanoBiT assay

N-terminal LgBit and C-terminal smBit construct was purchased from Promega and KRAS (full length) was cloned with *Xho* I and *Bgl* II to LgBit and CRAF Ras binding domain (1-149) was cloned with *Eco*RI and *Bgl* II to SmBit. The construct was transfected into HeLa cells by employing transfection reagent (Polyethilenimine, PEI 25000, Sigma). For transfections, 1 μ g or 2 μ g of (12 well/6 well) plasmids were transfected into cells with 0.5mM of PEI reagent in 100 μ l or 200 μ l PBS. One day after transfection, cells were harvested and seeded into 96 well white plates (Greiner). After an additional day the medium was changed to serum free DMEM for 0 to 4 h containing either DMSO, rocaglamide (Active biochem), Flavaglines or ARS-1620 (Selleckchem, S8707). After pre-treatment, KRAS wild type transfected cells were stimulated with EGF for 30 min. NanoGlo assay was performed for the EGF stimulated KRAS wild type transfected cells or mutated KRAS transfected cells according to the manufacturer's instructions. The luminescence was measured using Tecan infinite (Tecan). One day after transfection, cells were harvested and transferred into 96 well white plate and kept for one day in the incubator. After incubation, NanoGlo assay was performed for the EGF stimulated KRAS WT transfected cells or mutated KRAS transfected cells according to the manufacturer's instructions. For co-transfection of plasmids and siRNAs, Lipofectamine 2000 reagent (Invitrogen) was employed. 1 μ l of siRNA (100 μ M), 0.25 μ g of LgBit and smBit plasmid was mixed in 125 μ l of opti-MEM and the mixture was added to 3 μ l lipofectamine 2000 containing Opti-MEM (125 μ l). After incubation, the solution was

used for transfection. siRNA for PHB1: 5'-CCCAGAAAUCACUGUGAAA-3, 5'-UUUCACAGUGAUUUCUGGG.

MTT assay

HCT-116, Calu-1, and ASPC-1 cells were seeded in 96 well plates at a concentration of 5×10^4 cells/ml. 50 μ l cell suspension were added into 96 well cell culture plates and cultured for one day. 50 μ l of compound containing growth medium was added to the well and the cells were cultured for additional 48 h. 10 μ l of MTT solution was added to the wells and incubated for 2 to 3 h. After incubation with MTT, solubilisation buffer was added and incubated overnight. MTT was measured at OD 570 nm.

Soft agar colony formation assay

1.5% agarose solution was mixed with 2x growth medium (20% FBS, with or without 100 nM rocaglamide) and placed with 1.5 ml of 0.75% agarose/1x growth medium in 6 well plates. To solidify agarose, plates were incubated at room temperature for at least 10 min. HCT-116 and ASPC-1 cells were diluted in 2x growth medium (20% FBS, with or without 100 nM rocaglamide) and mixed with 0.9% agarose solution. 1.5 ml of cell suspension in 0.45% agarose in 1x growth medium was added to the bottom agarose layer. The cells seeded in soft agar were cultured for 2 to 4 weeks followed by crystal violet staining. The images were taken using a ChemiDoc Touch (Bio-Rad) and the number of colonies was counted by Image J software. Soft agar colony formation assays were also performed in 96 well plates to simplify the quantification of colonies. In short, 50 μ l of 0.75% agarose/1x growth medium was added to the 96 well plate. Cell suspension was prepared in 1x growth medium and mixed with 0.75% agarose/1x growth medium (1:2 ratio, 75 μ l). 2500-5000 cells were seeded in each well and 100 μ l of growth medium was added to the solidified layer with compounds. After one week, 20 μ l of MTT solution was added to the well and incubated for 4 h. After incubation, the medium was removed and 175 μ l of solubilisation buffer was added and the plate was heated at 70°C followed by absorbance measurement.

Animal experiments

SP-C/rtTA (SP-C) mice (Tichelaar et al., 2000) were crossed to TetO-KRAS4bG12D (KRAS G12D) mice (Fisher et al., 2001). For transgene expression, mice were fed a doxycycline (DOX) diet for a total of 3.5 months. After two months, treatment with rocaglamide (2.5mg/kg, 3 times/week) was started and continued for 6 weeks. The

DOX diet was purchased from ssniff Spezialdiäten GmbH. C57BL/6J and B6129SF1/J mice were treated with rocaglamide (2.5mg/kg, 3 times/week) for 2 or 4 weeks respectively to address potential cytotoxicity on liver and kidney. For toxicity testing, blood of 2-4 weeks rocaglamide-treated mice was subjected to analysis of liver transaminases and kidney parameters. All animal experiments were approved by local authorities (National Investigation Office Rheinland-Pfalz, Approval ID: G15-1-064) and conducted according to the German Animal Protection Law.

FLIM-FRET

HEK 293 EBNA cells were seeded in 6-well or 12 well plates onto 16 mm sterile cover slips. The next day, cells were transfected by FuGENE HD transfection reagent (E2311, Promega) or jetPRIME (114-15, Polyplus) using a total of 2 µg plasmids for 6 well or 0.8 µg of plasmids for 12 well plates. For donor fluorophore lifetime samples, cells were transfected with only mGFP-tagged RAS G12V plasmid. In FRET pairs, cells were transfected with mGFP-tagged and mCherry-tagged RAS G12V plasmids at a ratio of 1:3. To monitor FRET between KRAS and PS, cells were co-transfected with pmGFP-Lact C2 and pmcherry-KRAS G12V at a ratio of 1:3. To monitor FRET between KRAS and PA, cells were co-transfected with pmGFP-KRAS G12V and pmRFP-Pass at a ratio of 1:3. 24 h after transfection, cells were treated with either 0.1% DMSO control or 25 or 50 nM rocaglamide for 24 h and fixed in 4% PFA for 12 min before mounting with Mowiol 4–88 (Sigma–Aldrich, Cat. No. 81381). The donor fluorophore lifetime was measured using a Lambert-Fluorescence Lifetime Imaging instrument (Groningen, The Netherlands) attached to a fluorescence microscope (Zeiss AXIO Observer D1) as previously described (Guzman et al., 2014). The percentage of the apparent FRET efficiency (E_{app}), was measured using the lifetimes of donor-acceptor pairs (τ_{DA}) of samples and the average donor lifetime (τ_D), based on the equation: $E_{app} = (1 - \tau_{DA} / \tau_D) \times 100\%$.

Nanobar-based RAS activation assay

The nanobar arrays with 250 nm width, 2 µm length, 300 nm height and 5 µm pitch were fabricated on a square quartz wafer by using electron-beam lithography (FEI Helios NanoLab) as previously reported (Zhao et al., 2017). For cell culture and live-cell imaging, the nanobar chips were immersed in Chromium Etchant (Sigma-Aldrich) overnight to remove the Cr mask of nanobars, then attached to hole-punched

40 x 11 mm tissue culture dishes (TPP). Prior to cell culture, the nanobar-chip bottom dish was treated with air plasma for 5 mins and coated with 2 mg/ml gelatine (Sigma-Aldrich) for 30 mins at room temperature. 5×10^4 U-2OS cells were seeded in the chip bottom dish and maintained in the complete DMEM supplemented with GlutaMAX™ until 70%-90% confluency for DNA transfection, drug treatment, live cell imaging and immunostaining was reached. Imaging of KRAS-transfected cells w/o rocaglamide treatment on nanobar arrays was performed with laser scanning confocal microscopy (Zeiss LSM 800 with Airyscan) at 100x/1.4 oil objective. Each image had a resolution of 512×512 pixels, with a pixel size of 124 nm and a bit depth of 16. To quantify the curved nanobar-end preferred distribution of each protein with or without drug treatment, the background intensity of each image was subtracted by a rolling ball algorithm at 3.5-pixel radius in Fiji NIH (Schindelin et al., 2012) and the intensity ratio of nanobar-end to nanobar-center was measured and calculated using a custom-written Matlab code derived from previously reported work (Zhao et al., 2017).

Immunogold labelling and quantification of RAS clusters

Intact apical plasma membrane (PM) sheets of BHK cells expressing GFP-tagged RAS oncogenic mutants, GFP-KRAS.G12V, GFP-HRAS.G12V or GFP-NRAS.G12V, were attached to copper EM grids. After fixation with 4% paraformaldehyde (PFA) and 0.1% glutaraldehyde, the PM sheets were immunolabeled with 4.5 nm gold nanoparticles conjugated to anti-GFP antibody, negative-stained with uranyl acetate and embedded in methyl cellulose. The PM sheets with the gold-labeled GFP-RAS mutants were imaged using transmission EM at a magnification of 100,000x. ImageJ was used to assign coordinates to each gold particle. Within a selected $1 \mu\text{m}^2$ area on intact PM sheets, the spatial distribution of gold particles was calculated using Ripley's K-function, which tests a null hypothesis that all gold in a selected area are distributed randomly:

$$K(r) = An^{-2} \sum_{i \neq j} w_{ij} 1(\|x_i - x_j\| \leq r) \quad (\text{Eq. A})$$

$$L(r) - r = \sqrt{\frac{K(r)}{\pi}} - r \quad (\text{Eq. B})$$

where $K(r)$ denotes the univariate K-function for n particles in an area of A ; r is the length between 1 and 240 nm and has an increment of 1nm; $\|\cdot\|$ is Euclidean distance; where the indicator function of $1(\cdot) = 1$ if $\|x_i - x_j\| \leq r$ and $1(\cdot) = 0$ if $\|x_i - x_j\| > r$.

To correct a potential edge effect, w_{ij}^{-1} describes the portion of the circumference of a circle with the center at x_i and radius $\|x_i - x_j\|$. $K(r)$ is converted to $L(r) - r$, which is further normalized against the 99% confidence interval (99% C.I.). The 99% C.I. is estimated from Monte Carlo simulations. A $L(r) - r$ value of 0 describes a complete random distribution of gold. A $L(r) - r$ value above the 99% C.I. of 1 indicates statistical clustering. For each condition, at least 15 PM sheets were imaged, analyzed and pooled. Statistical significance was evaluated via comparing our calculated point patterns against 1000 bootstrap samples in bootstrap tests (Zhou and Hancock, 2015; Zhou et al., 2017).

RAS-PHB1 binding assay

HeLa cells were seeded at the density of 5×10^4 cells/ml in 6 well plate (2 ml). After transfection of the FLAG-KRAS, NRAS and HRAS G12D plasmid, cells were cultured for 2 days followed by DSP crosslink. RAS-overexpressing HeLa cells were washed with PBS twice and 750 μ l of PBS was added to the 6 well plate with DSP (1mM, 4% DMSO) at room temperature for 30 min. After incubation, the reaction was stopped with TBS (50 mM Tris-HCl pH 7.5, 150 mM NaCl) and washed with TBS. The cell lysate was prepared in active RAS pull-down buffer and the lysate was used for FLAG immunoprecipitation assay. 10 μ l of anti-FLAG M2 Affinity Gel (Sigma, A2220-5ML) was added to the lysate and rotated at 4°C for 1 h. After washing with binding buffer, SDS-PAGE and Western blotting was performed as described above.

Bimolecular fluorescent complementation (BiFC) assay

Full length PHB1 and KRAS G12D were cloned into the BiFC plasmid pair (Addgene #73636, #73637) which was kindly gifted by Darren Saunders (Croucher et al., 2016). The plasmid was transfected into HeLa cells as described before and the cells were harvested with Trypsin/EDTA solution. The cells were used for the FACS analysis.

Cellular Thermal Shift Assay (CETSA)

HEK-293T cells were harvested in 10% glycerol/PBS with protease inhibitor (Roche, EDTA-free). The protein concentration was adjusted to 0.5 μ g protein/ml and aliquoted to 1.5 ml tube, 30 μ l/tube with 200 nM of rocaglamide, FL42 or FL1 followed by an incubation on ice for 30 min. After incubation, the tubes were heated

on a heat block for 6 min and then transferred to an icebox. The lysate was centrifuged (13000 x rpm, 4°C, 15 min) and the supernatant was employed for SDS-PAGE and Western blotting.

siRNA transfection

2 µl of siRNA (100 µM) was mixed with 10 µl of SAINT-sRNA (Synvolux) in 200 µl of PBS and incubated for 10 min at room temperature. HeLa cells were harvested with 0.05% Trypsin/0.02% EDTA in PBS and seeded in 6 or 12 well cell culture plates at a concentration of 5×10^4 cells/ml in complete DMEM (2 ml for 6 well plate and 1 ml for 12 well plate). After one day, transfection reagent was added to the well and the cells were maintained in the incubator for 1 to 2 days. The medium was changed to serum-free DMEM and incubated at 37°C for 4 h with compound (100 nM). After starvation of the cells, they were stimulated with EGF (100 ng/ml) for 30 min. The cells were washed with PBS and used for active RAS pull down assay.

siRNA for PHB1: 5'-CCCAGAAAUCACUGUGAAA-3', 5'-UUUCACAGUGAUUUCUGGG. siRNA for CRAF: 5'-GGAUGUUGAUGGUAGUACATT-3', 5'-UGUACUACCAUCAACAUCAC-3'

Lipid binding assay

3xFLAG-CMV-14 with PHB1 full-length insert was transfected into HEK-293T for 2 days in 15cm diameter cell culture dishes. After overexpression, the cells were lysed in active RAS pull-down assay buffer and the 300 µl of anti-FLAG-M2 antibody immobilized agarose (Sigma) was added to the lysate. After 4 h of incubation at 4°C, the beads were washed with TBS (50 mM Tris-HCl pH 7.5, 150 mM NaCl) followed by elution with 100 µg/ml of 3xFLAG peptide in TBS. The elution fraction was used for further experiments. The lipid strip (Echelon, P-6002) was blocked with 3% BSA/TBST overnight at 4°C. The membrane was incubated in the same buffer with either 1:500 diluted FLAG-tagged PHB1 elution fraction with 10 µM of rocaglamide or with the same amount of DMSO followed by overnight incubation at 4°C. Finally, the membrane was washed and the FLAG-PHB1 was detected by HRP-conjugated anti-FLAG M2 antibody. The signal intensity was quantified by ImageJ software.

Acknowledgement:

KR would like to thank the excellent technical support of Stefanie Wenzel. We thank Prof. Frank McCormick for critical advice. Ulf Rapp for providing cell lines and Dr. Schonfeld for critical reading of the manuscript. Part of this work is supported through a DFG grant RA1739/8-1 to KR and CRC1292 (TP05). KR is a Heisenberg professor of the DFG and a GFK fellow. Financial support to W.Z. NTU Start-Up-Grant (M4082114) NTU-NNI Joint Grant (M4082292). Technical support to nanobar assay: Centre for Disruptive Photonic Technologies (CDPT) and and Nanyang NanoFabrication Centre (N2FC) of Nanyang Technological University.

Author Contributions: HY designed and performed the experiments, analyzed/interpreted data and prepared figures. Yinyin and Yongpen contributed to Nanobar experiments and HL contributed to immunogold labeling and EM experiments. FS performed FRET-FLIM analysis and HAH contributed to synthesis of flavaglines. SR performed animal experiments and EB provided the NSCLC mouse model and advised SB. YZ, DA, WZ and LD contributed to design, analysis, interpretation and co advised the study. KR contributed to the conception, design, analyzed/interpreted data and supervised the study. KR and HY wrote the manuscript with input from all authors.

References

- Abankwa, D., A.A. Gorfe, K. Inder, and J.F. Hancock. 2010. Ras membrane orientation and nanodomain localization generate isoform diversity. *Proc Natl Acad Sci U S A*. 107:1130-1135.
- Boussemart, L., H. Malka-Mahieu, I. Girault, D. Allard, O. Hemmingsson, G. Tomasic, M. Thomas, C. Basmadjian, N. Ribeiro, F. Thuaud, C. Mateus, E. Routier, N. Kamsu-Kom, S. Agoussi, A.M. Eggermont, L. Desaubry, C. Robert, and S. Vagner. 2014. eIF4F is a nexus of resistance to anti-BRAF and anti-MEK cancer therapies. *Nature*. 513:105-109.
- Browman, D.T., M.B. Hoegg, and S.M. Robbins. 2007. The SPFH domain-containing proteins: more than lipid raft markers. *Trends Cell Biol*. 17:394-402.
- Chu, J., W. Zhang, R. Cencic, P.B.F. O'Connor, F. Robert, W.G. Devine, A. Selznick, T. Henkel, W.C. Merrick, L.E. Brown, P.V. Baranov, J.A. Porco, Jr., and J. Pelletier. 2020. Rocaglates Induce Gain-of-Function Alterations to eIF4A and eIF4F. *Cell Rep*. 30:2481-2488 e2485.
- Croucher, D.R., M. Iconomou, J.F. Hastings, S.P. Kennedy, J.Z. Han, R.F. Shearer, J. McKenna, A. Wan, J. Lau, S. Aparicio, and D.N. Saunders. 2016. Bimolecular complementation affinity purification (BiCAP) reveals dimer-specific protein interactions for ERBB2 dimers. *Science signaling*. 9:ra69.
- Ebada, S.S., N. Lajkiewicz, J.A. Porco, Jr., M. Li-Weber, and P. Proksch. 2011. Chemistry and biology of rocaglamides (= flavaglines) and related derivatives from aglaia species (meliaceae). *Prog Chem Org Nat Prod*. 94:1-58.
- Fisher, G.H., S.L. Wellen, D. Klimstra, J.M. Lenczowski, J.W. Tichelaar, M.J. Lizak, J.A. Whitsett, A. Koretsky, and H.E. Varmus. 2001. Induction and apoptotic regression of lung adenocarcinomas by regulation of a K-Ras transgene in the presence and absence of tumor suppressor genes. *Genes Dev*. 15:3249-3262.
- Guzman, C., M. Solman, and D. Abankwa. 2014. Nanoclustering and heterogeneous membrane diffusion of Ras studied by FRAP and RICS analysis. *Methods Mol Biol*. 1120:307-326.
- Hancock, J.F., and R.G. Parton. 2005. Ras plasma membrane signalling platforms. *Biochemical Journal*. 389:1-11.
- Hobbs, G.A., C.J. Der, and K.L. Rossman. 2016. RAS isoforms and mutations in cancer at a glance. *J Cell Sci*. 129:1287-1292.
- Ihle, N.T., L.A. Byers, E.S. Kim, P. Saintigny, J.J. Lee, G.R. Blumenschein, A. Tsao, S. Liu, J.E. Larsen, J. Wang, L. Diao, K.R. Coombes, L. Chen, S. Zhang, M.F. Abdelmelek, X. Tang, V. Papadimitrakopoulou, J.D. Minna, S.M. Lippman, W.K. Hong, R.S. Herbst, Wistuba, II, J.V. Heymach, and G. Powis. 2012. Effect of KRAS oncogene substitutions on protein behavior: implications for signaling and clinical outcome. *J Natl Cancer Inst*. 104:228-239.
- Janes, M.R., J. Zhang, L.S. Li, R. Hansen, U. Peters, X. Guo, Y. Chen, A. Babbar, S.J. Firdaus, L. Darjania, J. Feng, J.H. Chen, S. Li, S. Li, Y.O. Long, C. Thach, Y. Liu, A. Zariw, T. Ely, J.M. Kucharski, L.V. Kessler, T. Wu, K. Yu, Y. Wang, Y. Yao, X. Deng, P.P. Zarrinkar, D. Brehmer, D. Dhanak, M.V. Lorenzi, D. Hu-Lowe, M.P. Patricelli, P. Ren, and Y. Liu. 2018. Targeting KRAS Mutant Cancers with a Covalent G12C-Specific Inhibitor. *Cell*. 172:578-589 e517.

- Khan, I., J.M. Rhett, and J.P. O'Bryan. 2020. Therapeutic targeting of RAS: New hope for drugging the "undruggable". *Biochim Biophys Acta Mol Cell Res.* 1867:118570.
- Kim, D.K., H.S. Kim, A.R. Kim, G.H. Jang, H.W. Kim, Y.H. Park, B. Kim, Y.M. Park, M.A. Beaven, Y.M. Kim, and W.S. Choi. 2013. The scaffold protein prohibitin is required for antigen-stimulated signaling in mast cells. *Science signaling.* 6:ra80.
- Liang, H., H. Mu, F. Jean-Francois, B. Lakshman, S. Sarkar-Banerjee, Y. Zhuang, Y. Zeng, W. Gao, A.M. Zaske, D.V. Nissley, A.A. Gorfe, W. Zhao, and Y. Zhou. 2019. Membrane curvature sensing of the lipid-anchored K-Ras small GTPase. *Life Sci Alliance.* 2.
- Merkwirth, C., and T. Langer. 2009. Prohibitin function within mitochondria: essential roles for cell proliferation and cristae morphogenesis. *Biochim.Biophys.Acta.* 1793:27-32.
- Mishra, S., S.R. Ande, and B.L. Nyomba. 2010. The role of prohibitin in cell signaling. *FEBS J.*
- Oh-Hashi, K., Y. Hirata, and K. Kiuchi. 2016. SOD1 dimerization monitoring using a novel split NanoLuc, NanoBit. *Cell Biochem Funct.* 34:497-504.
- Osman, C., M. Haag, C. Potting, J. Rodenfels, P.V. Dip, F.T. Wieland, B. Brugger, B. Westermann, and T. Langer. 2009. The genetic interactome of prohibitins: coordinated control of cardiolipin and phosphatidylethanolamine by conserved regulators in mitochondria. *The Journal of cell biology.* 184:583-596.
- Ostrem, J.M., and K.M. Shokat. 2016. Direct small-molecule inhibitors of KRAS: from structural insights to mechanism-based design. *Nature reviews. Drug discovery.* 15:771-785.
- Polier, G., J. Neumann, F. Thuaud, N. Ribeiro, C. Gelhaus, H. Schmidt, M. Giaisi, R. Kohler, W.W. Muller, P. Proksch, M. Leippe, O. Janssen, L. Desaubry, P.H. Krammer, and M. Li-Weber. 2012. The natural anticancer compounds rocaglamides inhibit the Raf-MEK-ERK pathway by targeting prohibitin 1 and 2. *Chem Biol.* 19:1093-1104.
- Rajalingam, K., C. Wunder, V. Brinkmann, Y. Churin, M. Hekman, C. Sievers, U.R. Rapp, and T. Rudel. 2005. Prohibitin is required for Ras-induced Raf-MEK-ERK activation and epithelial cell migration. *Nat.Cell Biol.* 7:837-843.
- Ribeiro, N., F. Thuaud, Y. Bernard, C. Gaidon, T. Cresteil, A. Hild, E.C. Hirsch, P.P. Michel, C.G. Nebigil, and L. Desaubry. 2012. Flavaglines as potent anticancer and cytoprotective agents. *J Med Chem.* 55:10064-10073.
- Ryan, M.B., F. Fece de la Cruz, S. Phat, D.T. Myers, E. Wong, H.A. Shahzade, C.B. Hong, and R.B. Corcoran. 2019. Vertical pathway inhibition overcomes adaptive feedback resistance to KRASG12C inhibition. *Clin Cancer Res.*
- Schindelin, J., I. Arganda-Carreras, E. Frise, V. Kaynig, M. Longair, T. Pietzsch, S. Preibisch, C. Rueden, S. Saalfeld, B. Schmid, J.Y. Tinevez, D.J. White, V. Hartenstein, K. Eliceiri, P. Tomancak, and A. Cardona. 2012. Fiji: an open-source platform for biological-image analysis. *Nature methods.* 9:676-682.
- Simanshu, D.K., D.V. Nissley, and F. McCormick. 2017. RAS Proteins and Their Regulators in Human Disease. *Cell.* 170:17-33.

- Solman, M., A. Ligabue, O. Blazevids, A. Jaiswal, Y. Zhou, H. Liang, B. Lectez, K. Kopra, C. Guzman, H. Harma, J.F. Hancock, T. Aittokallio, and D. Abankwa. 2015. Specific cancer-associated mutations in the switch III region of Ras increase tumorigenicity by nanocluster augmentation. *eLife*. 4:e08905.
- Thuaud, F., Y. Bernard, G. Turkeri, R. Dirr, G. Aubert, T. Cresteil, A. Baguet, C. Tomasetto, Y. Svitkin, N. Sonenberg, C.G. Nebigil, and L. Desaubry. 2009. Synthetic analogue of rocaglaol displays a potent and selective cytotoxicity in cancer cells: involvement of apoptosis inducing factor and caspase-12. *J Med Chem*. 52:5176-5187.
- Thuaud, F., N. Ribeiro, C. Gaididon, T. Cresteil, and L. Desaubry. 2011. Novel flavaglines displaying improved cytotoxicity. *J Med Chem*. 54:411-415.
- Thuaud, F., N. Ribeiro, C.G. Nebigil, and L. Desaubry. 2013. Prohibitin ligands in cell death and survival: mode of action and therapeutic potential. *Chem Biol*. 20:316-331.
- Tichelaar, J.W., W. Lu, and J.A. Whitsett. 2000. Conditional expression of fibroblast growth factor-7 in the developing and mature lung. *J Biol Chem*. 275:11858-11864.
- Tsai, F.D., M.S. Lopes, M. Zhou, H. Court, O. Ponce, J.J. Fiordalisi, J.J. Gierut, A.D. Cox, K.M. Haigis, and M.R. Philips. 2015. K-Ras4A splice variant is widely expressed in cancer and uses a hybrid membrane-targeting motif. *Proc Natl Acad Sci U S A*. 112:779-784.
- Yurugi, H., F. Marini, C. Weber, K. David, Q. Zhao, H. Binder, L. Desaubry, and K. Rajalingam. 2017. Targeting prohibitins with chemical ligands inhibits KRAS-mediated lung tumours. *Oncogene*.
- Yurugi, H., S. Tanida, A. Ishida, K. Akita, M. Toda, M. Inoue, and H. Nakada. 2012. Expression of prohibitins on the surface of activated T cells. *Biochem Biophys Res Commun*. 420:275-280.
- Zhao, W., L. Hanson, H.Y. Lou, M. Akamatsu, P.D. Chowdary, F. Santoro, J.R. Marks, A. Grassart, D.G. Drubin, Y. Cui, and B. Cui. 2017. Nanoscale manipulation of membrane curvature for probing endocytosis in live cells. *Nat Nanotechnol*. 12:750-756.
- Zhou, Y., and J.F. Hancock. 2015. Ras nanoclusters: Versatile lipid-based signaling platforms. *Biochim Biophys Acta*. 1853:841-849.
- Zhou, Y., P. Prakash, H. Liang, K.J. Cho, A.A. Gorfe, and J.F. Hancock. 2017. Lipid-Sorting Specificity Encoded in K-Ras Membrane Anchor Regulates Signal Output. *Cell*. 168:239-251 e216.

Figures

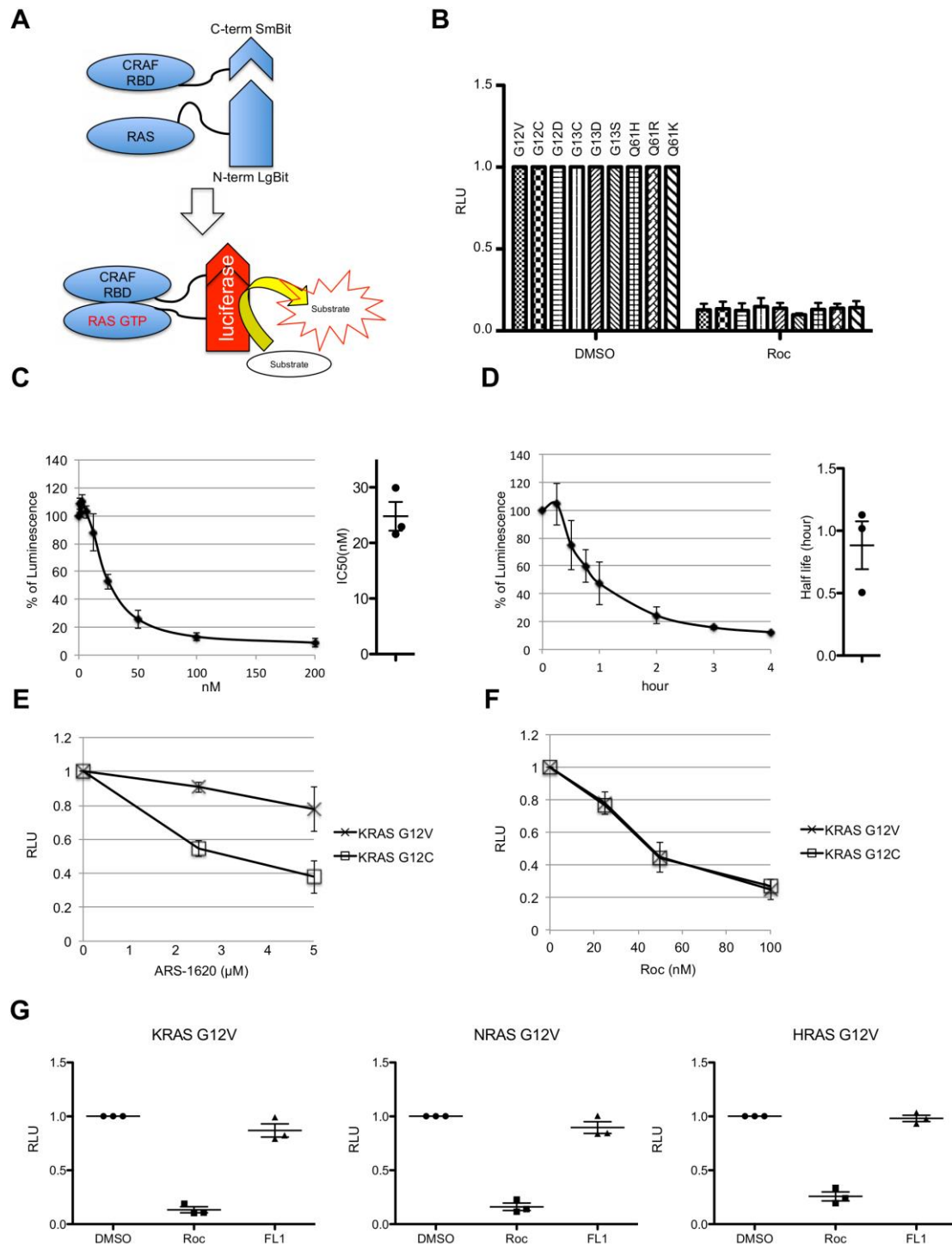


Figure 1 Rocaglamide treatment inhibit KRAS activation

(A) The cartoon shows the NanoBit system to monitor the RAS-GTP loading. (B) NanoBit assay for the KRAS GTP-loading was performed in HeLa cells transfected with LgBit-KRAS and SmBit-CRAF-RBD. Cells were treated with rocaglamide (100 nM) for 4 h in serum-free DMEM. After incubation, the substrate for NanoLuc was

added, and the luminescence was measured in a multiplate reader. Data were normalized to cells transfected with the indicated mutant and exposed to DMSO for 4 h. Shown are relative luminescence unit (RLU) and the value from DMSO-treated cells was taken as 1. The bars represent mean \pm SEM from 3 independent experiments. **(C)** IC₅₀ of rocaglamide was calculated from NanoBit assay using cells expressing LgBit-KRAS4B-G12V and SmBit-CRAF-RBD. Transfected cells were exposed to the indicated concentrations of rocaglamide for 4 h. IC₅₀ was calculated by one-phase decay equation in Prism5. The bars represent mean \pm SEM, from 3 independent experiments. **(D)** The NanoBiT assay for the KRAS4B G12V and CRAF-RBD was performed in order to obtain the half-life of the compound at the concentration of 100 nM. After transfection and the seeding to the white plate, cells were treated with rocaglamide at different time points. The data were evaluated by Prism5 software and half-life was calculated by one-phase decay equation in Prism5. The bars represent mean \pm SEM, from 3 independent experiments. **(E, F)** NanoBiT assay for KRAS4B and CRAF-RBD was performed as **C** and **D** in different concentration of the compounds ARS-1620 (KRAS G12C inhibitor) was used to test the system and also to compare with rocaglamide(Roc) treatment in this assay. Each plot shows the average and the error bars indicated \pm SD from 3 independent experiments. Shown are relative luminescence unit (RLU) and the value from DMSO-treated cells was set to 1. **G** NanoBiT assay for KRAS4B, NRAS and HRAS G12V was performed as shown in **B**. FL1 was used as a control compound. The RLU value of DMSO-treated cells was set to 1 and each plot indicates the value from 3 independent experiments. The bars represent mean \pm SEM.

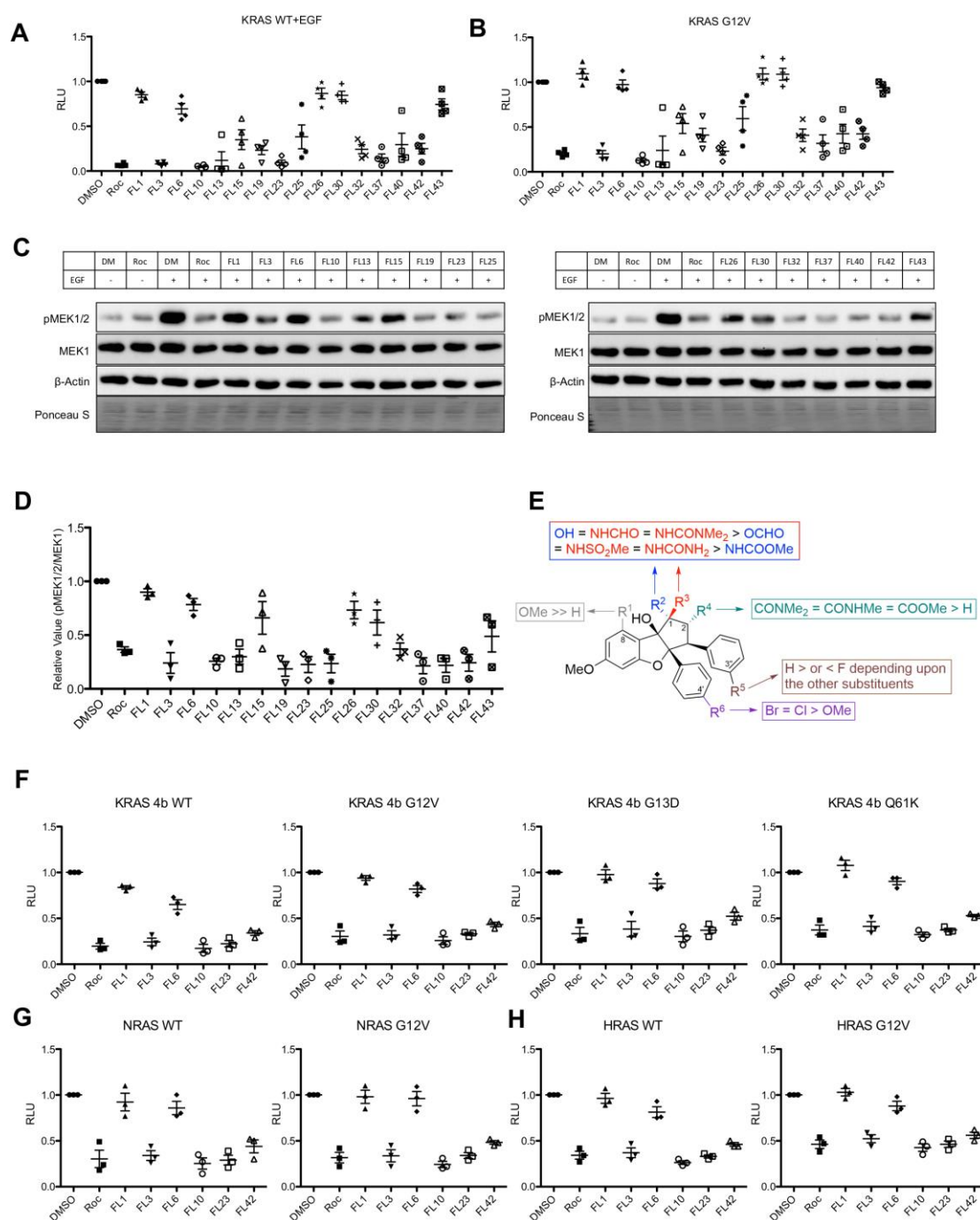


Figure 2 A subset of flavaglines inhibit RAS-GTP loading and MEK1/2 activation

(A) Different flavaglines (100 nM) were used for the RAS activation assay with NanoBiT system for KRAS and CRAF-RBD. For KRAS WT, cells were stimulated with EGF for 30 min after 4 h incubation with flavaglines. (B) For KRAS G12V mutation, the cells were treated with flavaglines for 4 h before adding the substrate. The value of DMSO-treated cells was set to 1 and each plot shows the relative value

from 4 independent experiments. The bars represent mean \pm SEM. (C) HeLa cells were treated with flavaglines for 4 h and stimulated with EGF for 30 min followed by SDS-PAGE to check the phosphorylation of MEK1/2. The result from one representative experiment is shown. (D) The panel depicts the quantification of Western blotting from 3 independent experiments. The value of DMSO-treated cells was set to 1 and each plot shows the relative value from 4 independent experiments. The bars represent mean \pm SEM. (E) SAR analysis was done based on the efficiency of inhibition of KRAS GTP-loading. (F, G, H) NanoBiT assay for KRAS4B G12V, G13D and Q61K (F), NRAS G12V (G) and HRAS G12V (H) was performed as shown in Figure 1 B. Several flavaglines were used for the assay at the concentration of 100 nM and the cells were treated with respective compounds for 4 h in serum-free medium. DMSO-treated cells served as control. In each plot values from 3 independent experiments are shown. The bars represent mean \pm SEM.

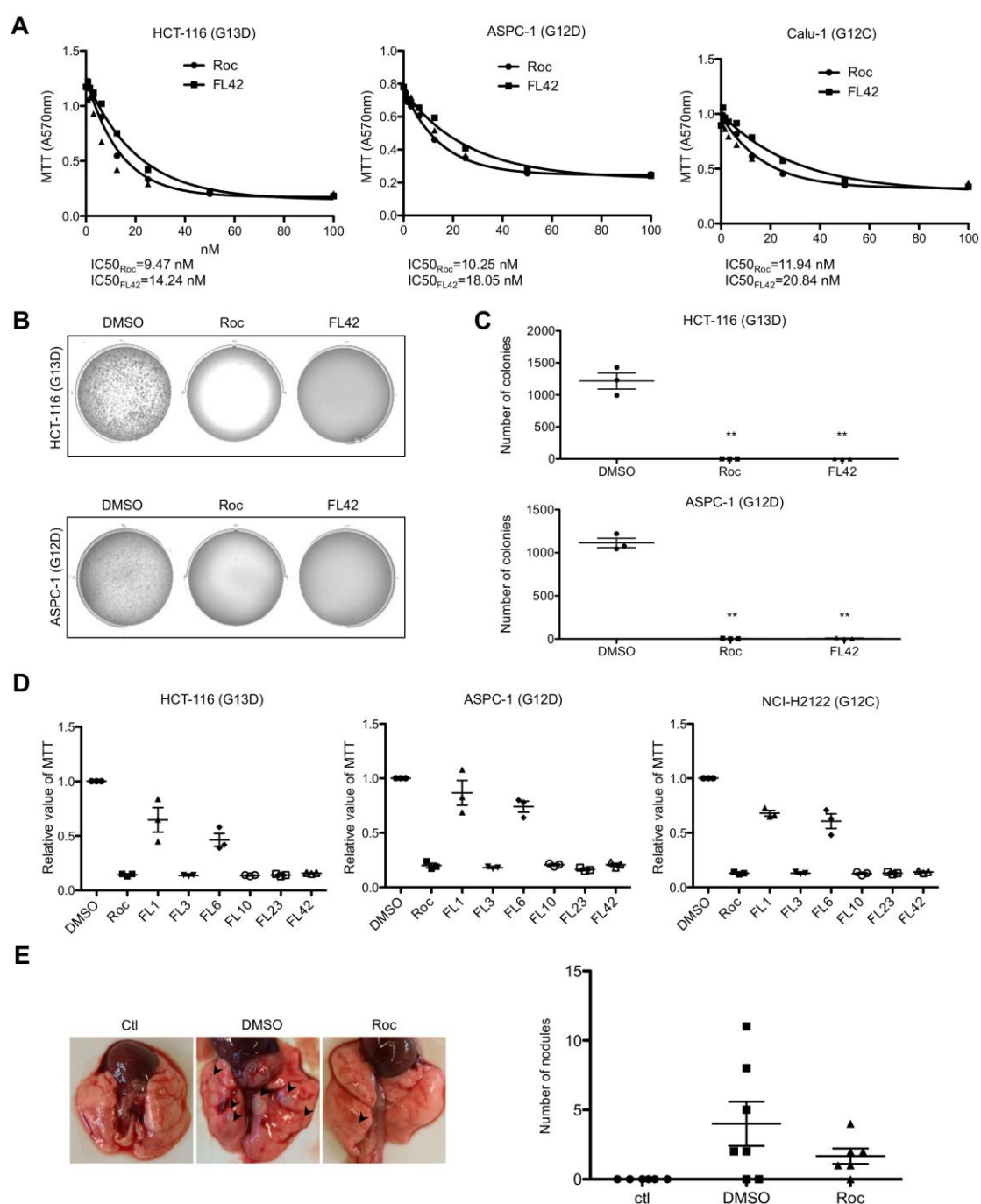


Figure 3 A subset of flavaglines inhibit cell growth in vitro and in vivo

(A) Cells with the indicated KRAS mutations were treated with rocaglamide or FL42 for 24 h and cell viability was evaluated by MTT assay. IC₅₀ was calculated by one-phase decay equation in Prism5. The bars represent mean ± SEM, from 3 independent experiments. (B, C) HCT-116 and ASPC-1 cells were used for the soft agar colony formation assay. After the assay, the colonies were stained with crystal violet and counted using ImageJ software. The bars represent mean ± SEM. Statistical significance was evaluated by Welch's t test in Excel (** p < 0.01). (D) Soft agar

colony formation assay was performed in 96 well plates as indicated in the methods section. After one week of cell culture in soft agar with compounds (100 nM), cells were treated with MTT and solubilized after 4 h of incubation. The value was obtained by measuring of absorbance (570 nm). Relative values were shown in the figure and the value from DMSO treated cells served as control. The bars represent mean \pm SEM. **(E)** DOX diet was given to the animals for 2 months. Then animals were treated with either rocaglamide (Roc, 2.5 mg/kg) or DMSO by intraperitoneal injections every 2 days for 6 weeks. Representative lung images are shown in the upper panel. Nodules (arrowheads) were counted for all lungs. Each dot plot indicates the data from one individual animal and the bars represent mean \pm SEM.

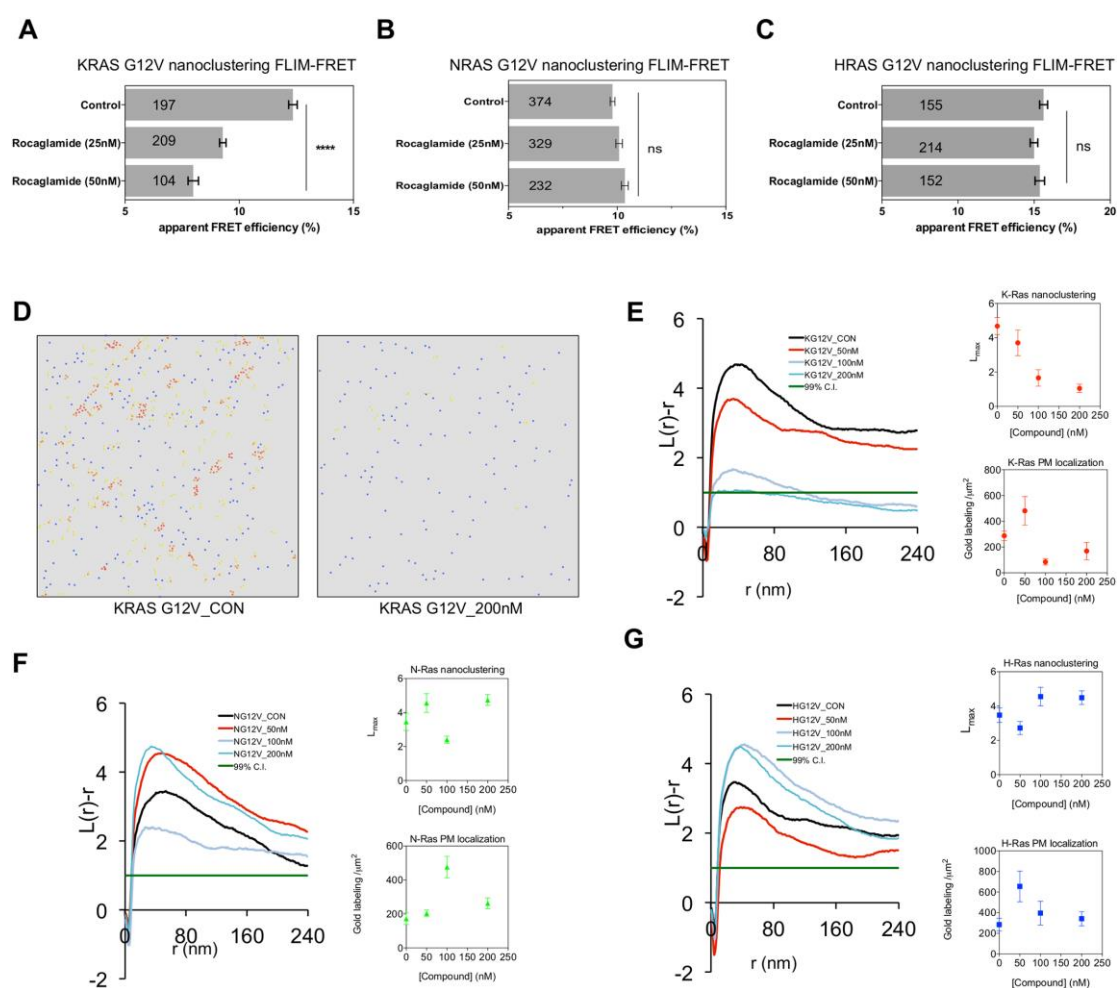


Figure 4 Rocaglamide treatment inhibits KRAS nano-clustering

(A-C) Effect of rocaglamide on KRAS G12V, HRAS G12V and NRAS G12V nanoclustering-FRET. HEK-293 EBNA cells were transfected with pmGFP-tagged KRAS G12V or HRAS G12V or NRAS G12V (1 μ g) for donor fluorophore lifetimes. For cells expressing the FRET pairs, cells were co-transfected with pmGFP-KRAS G12V (0.5 μ g) and pmCherry-KRAS G12V (1.5 μ g), or pmGFP-HRAS G12V (0.5 μ g) and pmCherry-HRAS G12V (1.5 μ g), or pmGFP-NRAS G12V (0.5 μ g) and pmCherry-NRAS G12V (1.5 μ g). After 24 h, cells were treated with 0.1% DMSO control or 25 nM or 50 nM of rocaglamide. After 24 h of treatment, cells were fixed with 4% PFA. Numbers on the bars indicate number of analysed cells. Statistically significant differences between control and treated samples were examined using one-way ANOVA complemented with Tukey's comparison (significant; *** $p < 0.0001$; ns, not significant). The bars represent mean values \pm SEM from 3 independent biological experiments. (D) A 1 μ m² area of an intact apical PM sheet of a BHK cell expressing GFP-KRAS.G12V is shown with no treatment (CON) or with 200nM

rocaglamide. In each image, gold particles are color-coded to indicate the extent of clustering: blue = monomer; yellow = dimer; orange = trimer; red = higher ordered multimers. **(E)** Univariate K-function analysis calculates the extent of nanoclustering of gold particles in the EM images. The extent of nanoclustering, $L(r) - r$, was plotted against the length scale r in nanometers. $L(r) - r$ values above the 99% C.I. value of 0 indicate statistically significant clustering. The peak $L(r) - r$ value, termed as L_{max} , describes the optimal clustering. The number of gold particles within the $1\mu\text{m}^2$ PM area was counted to estimate the extent of PM localization of GFP-KRAS.G12V. **(F)** For gold-labeled GFP-HRAS.G12V, the extent of nanoclustering, $L(r) - r$, was plotted against the length scale r in nanometers. The optimal clustering L_{max} , or gold numbers, is shown as a function of different Roc concentrations. **(G)** For gold-labeled GFP-NRAS.G12V, the extent of nanoclustering, $L(r) - r$, was plotted against the length scale r in nanometers. The optimal clustering L_{max} , or gold numbers, is shown as a function of different Roc concentrations. **(D-G)** For each condition, at least 15 EM images were imaged, pooled and calculated. All data are shown as mean \pm SEM. For the clustering analysis, statistical analysis was conducted via comparing our point pattern with 1000 bootstrap samples in bootstrap tests. For gold number counting, one-component ANOVA was used to evaluate the statistical significance.

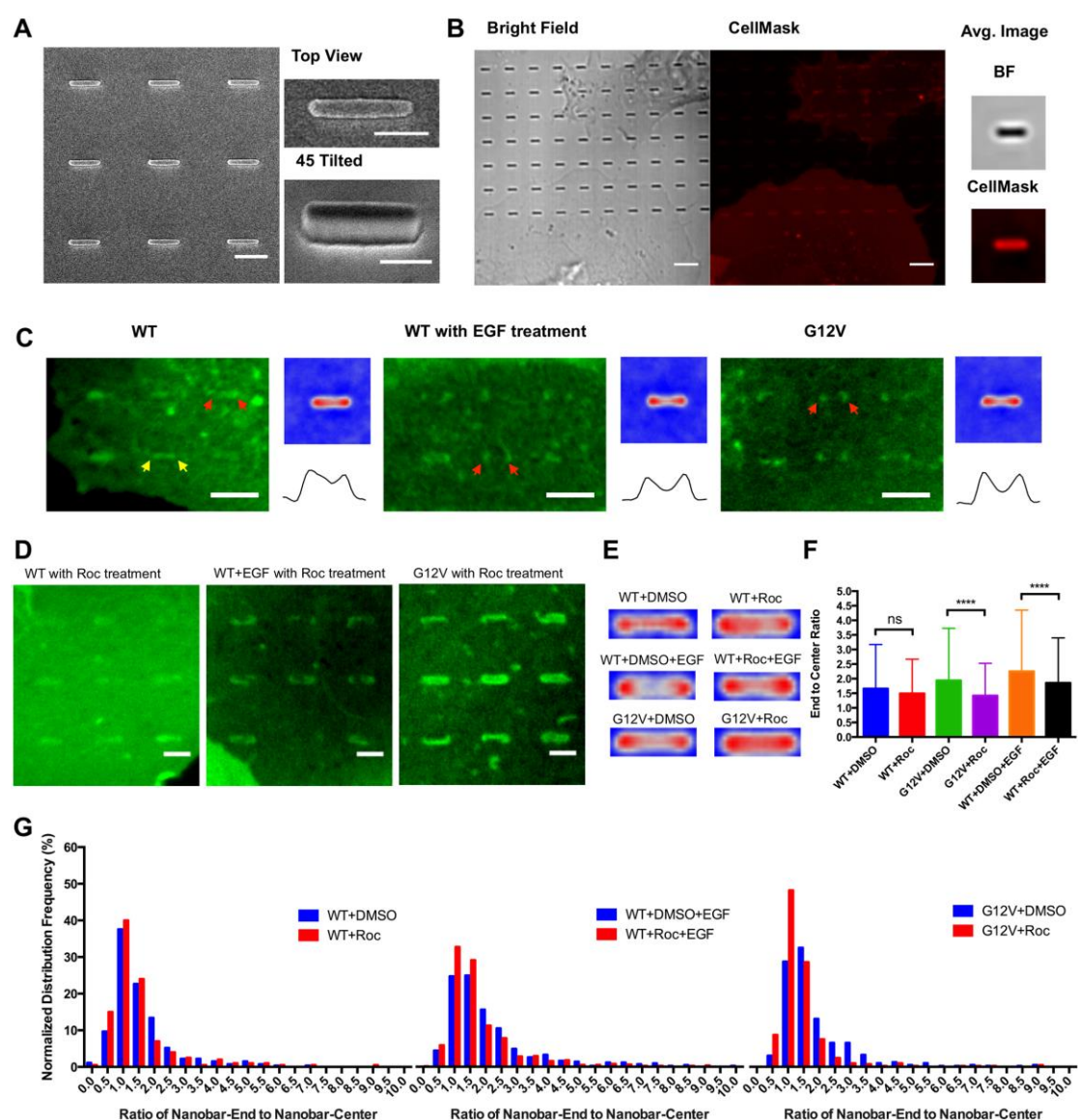


Figure 5 Rocaglamide treatment inhibits KRAS curvature response

(A) SEM images of a nanobar array showing individual nanobars with 250 nm width, 2 μm length, 300 nm height and 5 μm pitch. (left, scale bar: 2 μm, right, scale bar: 1 μm). (B) When U-2OS cells were cultured on gelatine-coated nanobar arrays, CellMask Deep Red staining showed that plasma membrane wrapped evenly around the nanobar. Scale bar: 5 μm. (C) U-2OS cells transfected with KRAS-WT-GFP were cultured on nanobar arrays. The confocal image showed that KRAS-WT mostly distributed evenly along the nanobar (yellow arrow), similar to CellMask, seen as B. While it may accumulate weakly at the curved nanobar end (red arrow). After EGF treatment, KRAS-WT accumulated strongly at the ends of the nanobars (red arrow). U-2OS transfected with KRAS mutation, G12V-GFP, showed that G12V also had

strong preference to accumulate at the ends of the nanobars (red arrows), similar to WT with EGF treatment. Averaged images of WT, G12V and WT with EGF treatment on 744-1052 nanobars were shown. Scale bar: 5 μ m. **(D)** U-2OS cells transfected with KRAS WT or KRAS G12V were treated with rocaglamide (Roc) for 4 h before imaging. For the EGF-induced KRAS group, cells were pre-treated with rocaglamide (Roc) for 4 h before EGF stimulation overnight. Rocaglamide (Roc) showed effect on inhibiting KRAS's preference to curved ends of the nanobars. Scale bar: 2 μ m. **(E)** Averaged images of KRAS+DMSO, KRASG12V+DMSO, KRAS+DMSO+EGF and their rocaglamide (Roc) treatments on 86-417 nanobars. **(F)** End to center intensity ratios of each protein/treatment were quantified by averaging over 200-784 data points. Error bar represents SEM. Statistical significance of WT vs. G12V, WT vs. WT +EGF, G12V vs. WT+EGF, WT+Roc vs. WT+DMSO, G12V+Roc vs. G12V+DMSO, and WT+DMSO+EGF vs. WT+Roc+EGF were evaluated by unpaired Kolmogorov-Smirnov test. p-value: ****<0.0001, ** < 0.05, ns>0.05. **(G)** Frequency distribution of end to center ratio of each protein w/wo rocaglamide (Roc) treatment indicated that KRAS maintained its distribution with peak at 1.0 bin center no matter with or without rocaglamide treatment. However, EGF-induced KRAS shifted back to distribution with 1.0 peak after rocaglamide (Roc) treatment compared to distribution of EGF-induced KRAS WT with peak at 1.5. KRAS G12V also showed left-shift to 1.0 with rocaglamide treatment, while KRAS G12V+DMSO showed its highest frequency at 1.5 bin center. The significant difference of EGF-induced KRAS with and without rocaglamide treatment or KRAS G12V with and without rocaglamide showed that rocaglamide performed strongly inhibitive effect on EGF-induced KRAS WT and KRAS G12V clustering preference at curved nanobar ends.

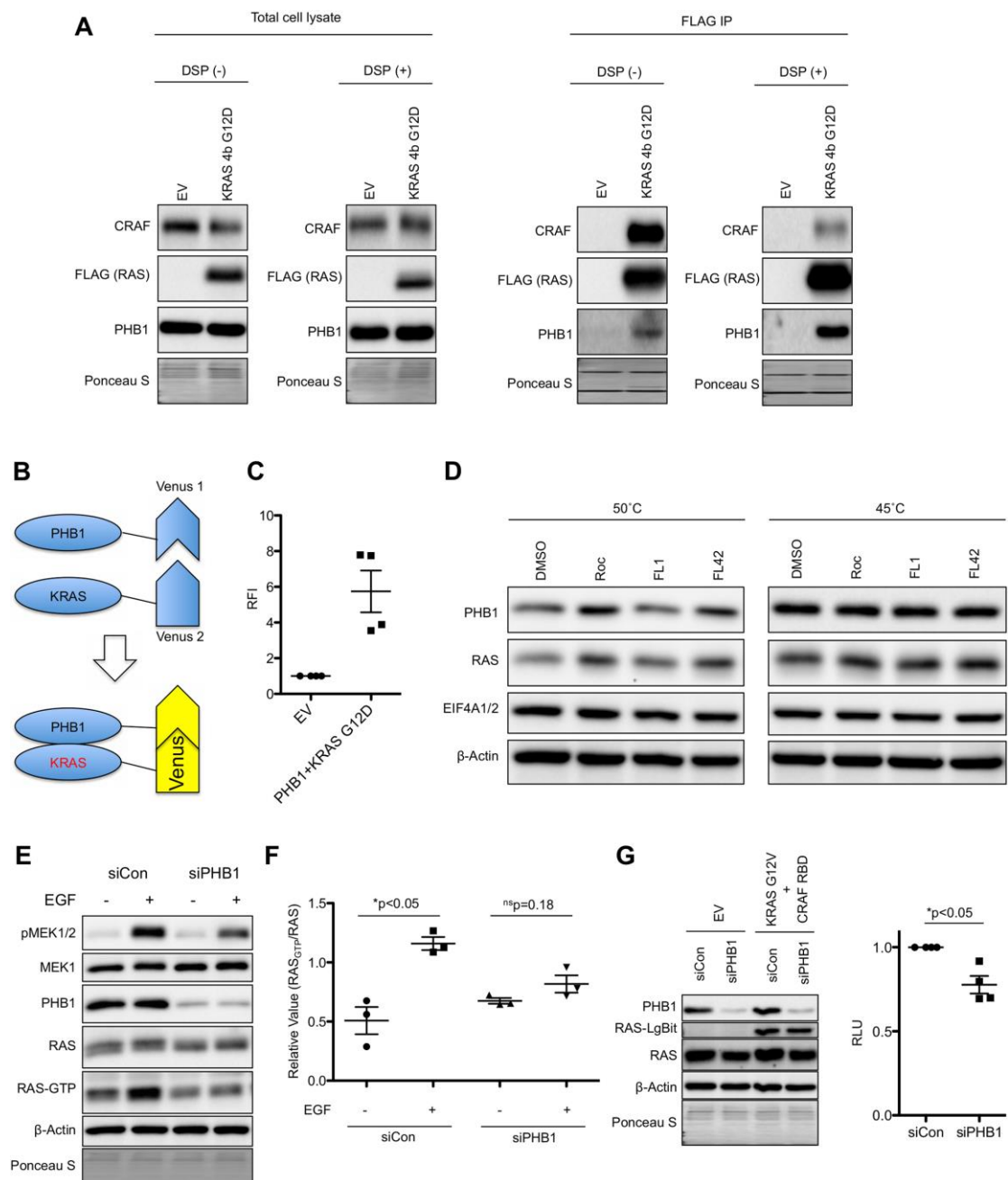


Figure 6 The role of PHB1 in KRAS activation

(A) Cells were transfected with KRAS G12D plasmid and after 2 days, the cell were treated with DSP for 30 min. After the reaction, cells were harvested and the lysate was obtained for the immunoprecipitation (IP). After IP, the sample was subjected to SDS-PAGE followed by Western blotting analysis. (B) The cartoon shows the BiFC system to monitor the interaction between KRAS and PHB1. (C) HeLa cells were transfected with PHB1 and KRAS BiFC pair. After 24 h, cells were harvested and FACS analysis was performed to check the level of YFP fluorescent signal. Dot blot shows the mean fluorescent intensity (MFI) from 4 independent experiments from each BiFC pair.

The bars represent mean \pm SEM and the value from empty vector control (EV) was taken as 1. **(D)** Cellular Thermal shift assay was performed using HEK-293T cell lysate. The lysate was prepared in 10% glycerol/PBS with proteinase inhibitor and incubated with 200 nM rocaglamide (Roc), FL1 or FL42 for 30 min on ice. After incubation, the cells were heated at 45 or 50°C for 6 min and then cooled on ice. After centrifugation, the supernatant was subjected to SDS-PAGE and Western blotting. **(E)** HeLa cells were transfected with siRNAs against PHB1 for 48 h followed by the stimulation with EGF (100 ng/ml) after 4 h of serum starvation. After stimulation, the cells were used for active RAS pull down assay. The sample was subjected to SDS-PAGE and Western blotting. **(F)** Dot plot shows the relative values of GTP-loaded RAS against total RAS from 3 independent experiments. The bars represent mean \pm SEM. Statistical significance was evaluated by Welch's t test in Excel. **(G)** NanoBiT for KRAS G12V and CRAF-RBD with siRNA against PHB1. The NanoBiT plasmid and siRNA was co-transfected to HeLa cells and NanoBiT assay was performed after 2 days from transfection. The left panel shows a representative image of Western blotting. The value from positive control pair from Promega (LgBit-PRKAR2A and SmBit-PRKACA) was used for normalization of the NanoBiT assay as siPHB1 transfection slightly inhibited the cell growth. Relative value was obtained from 4 independent experiments and the value from siCon was set to 1. The bars represent mean \pm SEM. Statistical significance was evaluated by Welch's t test in Excel.

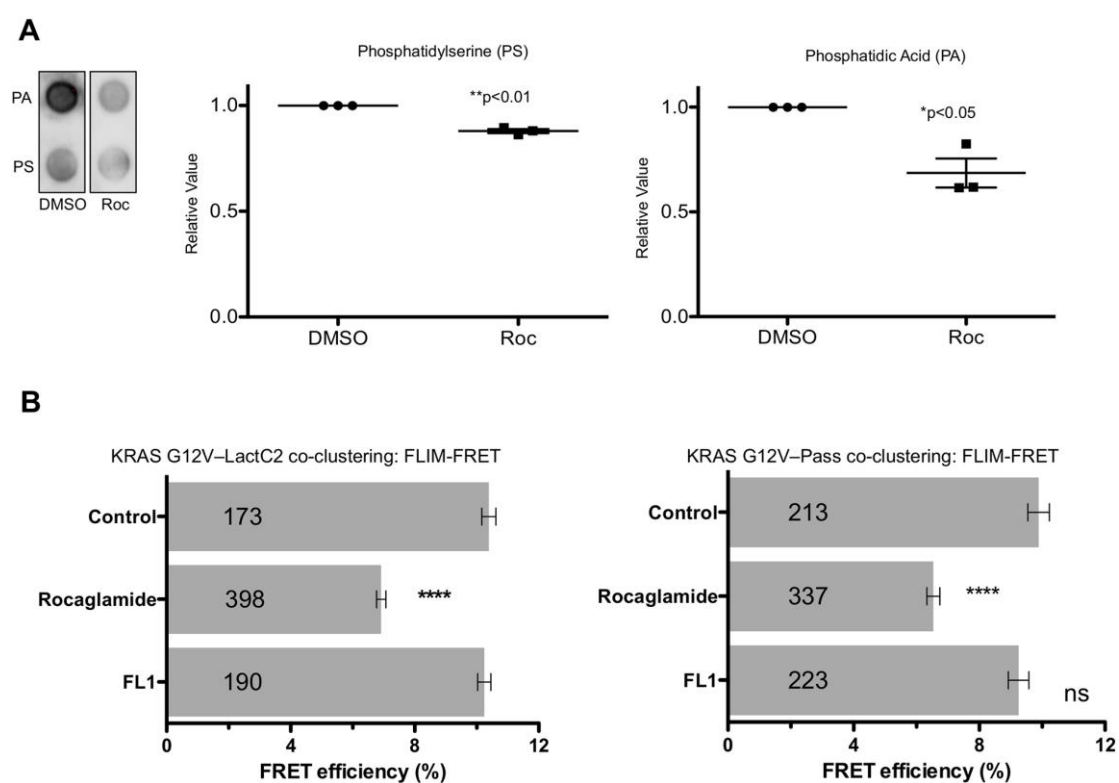


Figure 7 Rocaglamide treatment alters phospholipid affinity of PHB1 and KRAS

(A) Purified PHB1 was used for the lipid strip binding assay. The lipid membrane was incubated with PHB1 protein overnight either with rocaglamide (10 μ M) or DMSO. The signal intensity of the dot plot was obtained by Image J software and the data from 3 different experiments are shown as dot plots. The bars represent mean values \pm SEM and the Welch's t-test was applied for the p-value. (B) Effect of rocaglamide on KRAS G12V/LactC2 (left) and KRAS G12V/Pass (right) co-clustering. For KRAS G12V/LactC2 FRET, HEK 293 EBNA cells were transfected with mGFP-LactC2 to measure the lifetime of donor fluorophore and for the FRET pair, cells were transfected with mGFP-LactC2 and mCherry-KRAS G12V in ratio of 1:3. For KRAS G12V/Pass FRET pair, cells were transfected with mGFP-KRAS G12V to measure the lifetime of GFP only and for the FRET pair, cells were transfected with mGFP-KRAS G12V and mCherry-PASS in ratio of 1:3. Cells were treated with 0.1% DMSO control, 25 nM rocaglamide or FL1 for 24 h. Cells were fixed in 4% PFA. The apparent FRET efficiency was calculated from FLIM data (mean \pm SEM, n= 3). The numbers in the bars indicate the number of analyzed cells. Statistical significance of differences between control and treated cells were examined using one-way ANOVA tests (n.s., not significant; **** p<0.0001).

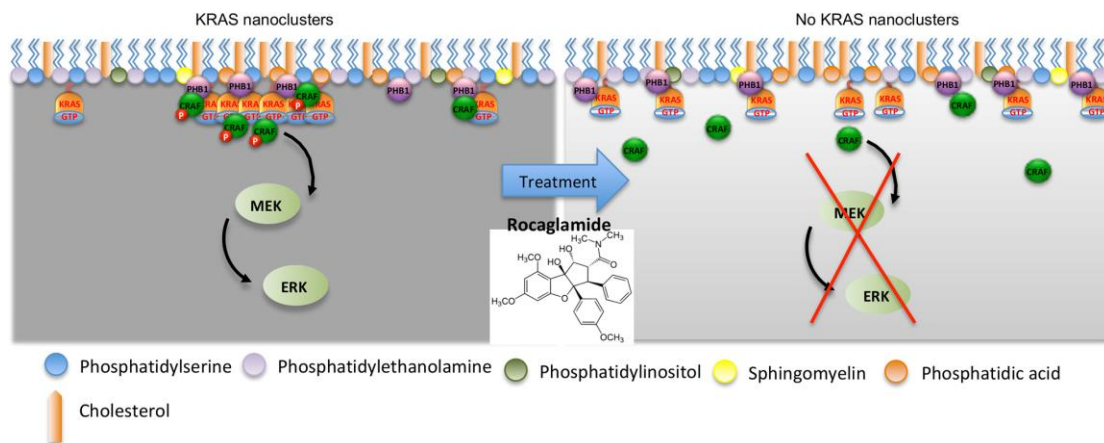


Figure 8 Scheme illustrating the proposed mechanism of KRAS inhibition by flavaglines. Rocaglamide treatment interferes with the formation of the KRAS-PS/PA-PHB1 complex, which causes to the disruption of KRAS nanoclusters in the plane of the plasma membrane and consequently prevents effector binding.

Supplementary figure 1

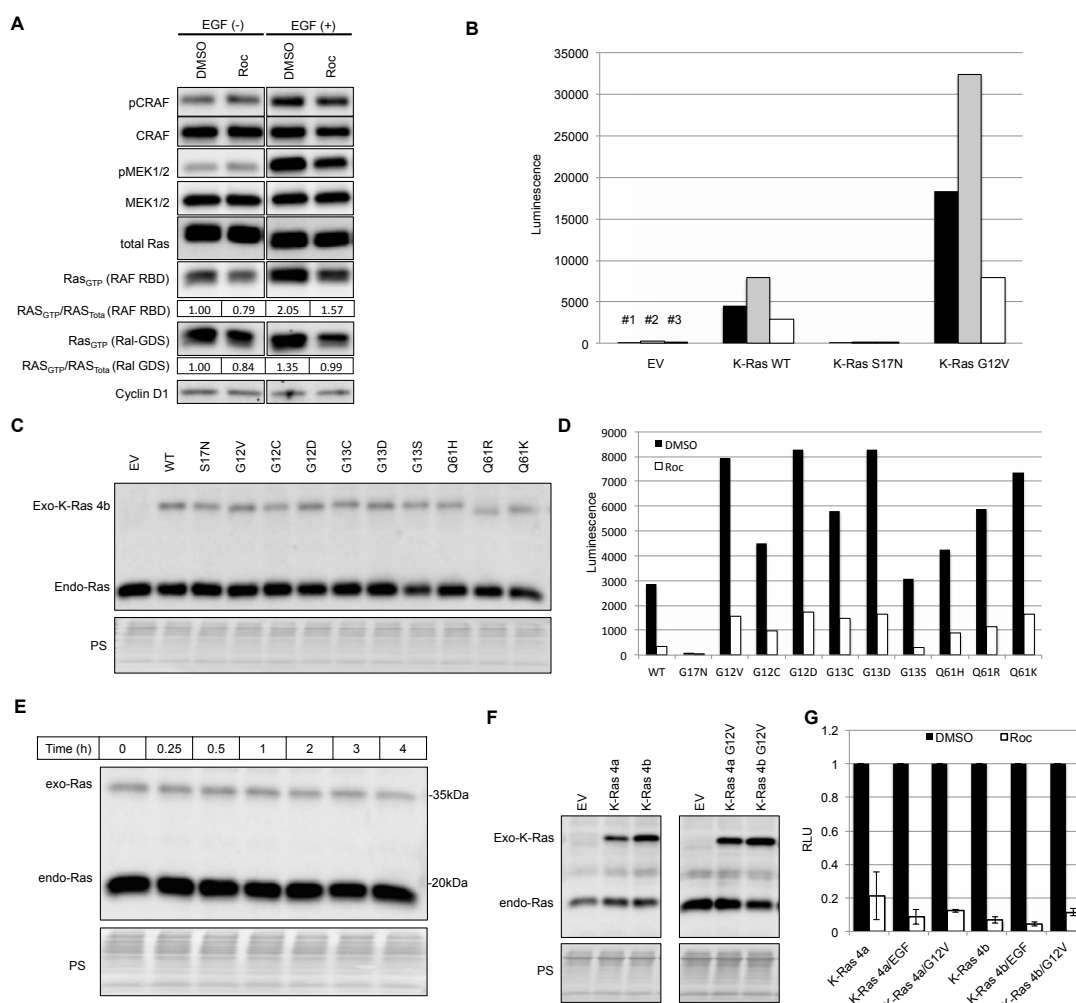


Figure S1 Validation of NanoBit assay for Ras activation

(A) HeLa cells were treated with rocaglamide (Roc, 200 nM) or DMSO for 1 h before the EGF stimulation. GTP-loaded Ras was pulled down with CRAF-RBD domain or RalGDS-RA domain and detected with pan-Ras antibody. the quantifications were presented below. The cyclin D levels was also monitored (B) The specificity of the Nanobit assay depicted in (Figure 1A) was evaluated by employing different mutants of the KRAS protein (C) The cells from a representative experiment presented in figure 1b were used for SDS-PAGE and Western blotting to check the expression level of LgBit-KRAS. (D) The bar graph shows the raw luminescence values from figure 1b. (E) The expression level of KRAS4A and B was checked by SDS-PAGE and Western blotting analysis. (F, G) NanoBit assay was performed for KRAS4A and KRAS4B in cells exposed to EGF (100 ng/ml) for 30 min. cell were used for SDS-PAGE and western blotting (F) and NanoBit assay (G). Data are presented are normalized to DMSO-pretreated, EGF-exposed cells expressing the indicated KRAS isoform. The bars represent mean \pm SD from 3 independent experiments.

Supplementary figure 2

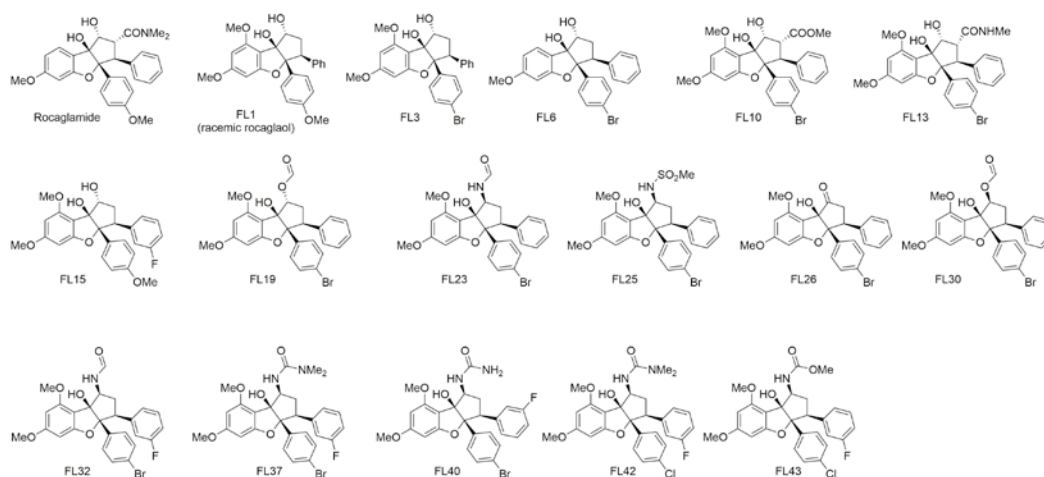


Figure S2 Structures of flavaglines. Shown are the chemical structures of different flavaglines employed in the screen.

Supplementary figure 3

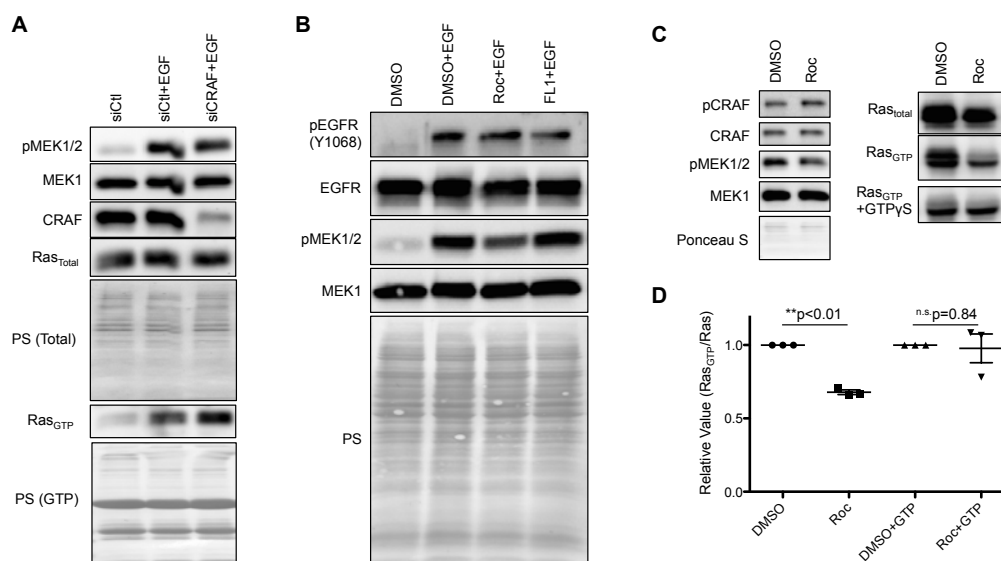


Figure S3 Mechanisms behind inhibition of RAS activation by Roc.

(A) HeLa cells were transfected with siRNAs targeting CRAF. After 2 days, the cells were cultured in serum-free medium for 4 h followed by EGF stimulation. After stimulation, the cells were lysed and the cell lysates were subjected to SDS-PAGE and Western blotting. **(B)** HeLa cells were treated with DMSO, Rocaglamide or FL1 for 4 h followed by EGF stimulation. The level of phosphorylated pEGFR, total EGFR, MEK1/2 and pMEK-1/2 were checked by Western blots. The ponceau staining (PS) of the entire membrane serves as a loading control **(C)** HeLa cells were transfected with KRAS G12V construct and treated with rocaglamide for 24 h. GTP- γ S was added to the lysate and active RAS was isolated by pull down assay with purified CRAF-RBD domain. **(D)** The dot plot shows the quantification of the Western blotting bands of RAS, DMSO-treated cells were taken as 1. The bars represent mean \pm SEM from 3 independent experiments.

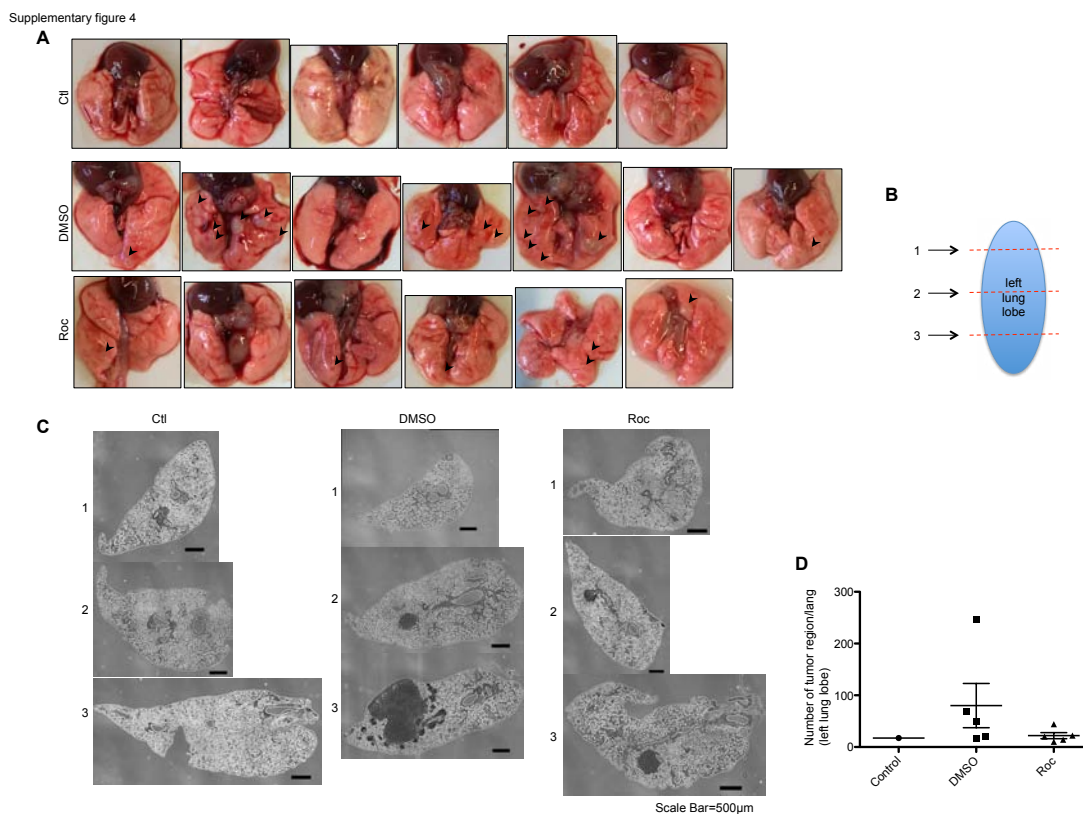


Figure S4 Rocaglamide treatment inhibit tumor growth in vivo

(A) Original Images of the mouse lung specimens from the figure 4E are shown. (B), (C) The sections were made every 0.1 mm of the whole left lung lobe and representative images from different regions of the H&E stained section are shown in C. Shown are images obtained under a DMi8 microscope with a 5X objective. (D) The tumour lesions were counted under the microscope. Tumor regions was calibrated by counting the number of tumour lesions from all the slides irrespective of the size of lesions. Each dot plot indicates the data from individual animals and the y-axis is the number of the tumour lesion containing areas from the all sections of one left lung lobe. The bars represent mean \pm SEM.

Supplementary figure 5

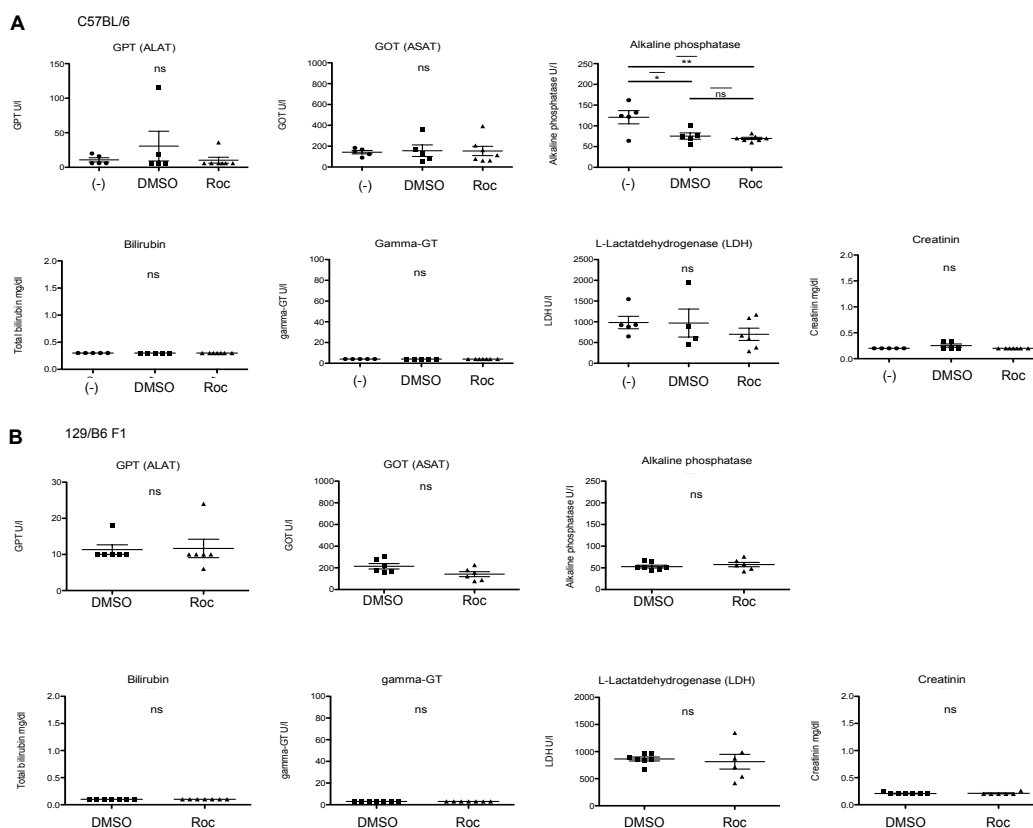


Figure S5 Profiling cytotoxicity of rocaglamide treatment in vivo (A, B) Roc or DMSO was injected intraperitoneally into the mice of 2 different mice strains with 99% of olive oil 3 times per week for 2-4 weeks. The cytotoxicity assay was performed for each animal as mentioned in the methods and each dot indicates individual animal. The bars represent mean \pm SEM.

Supplementary figure 6

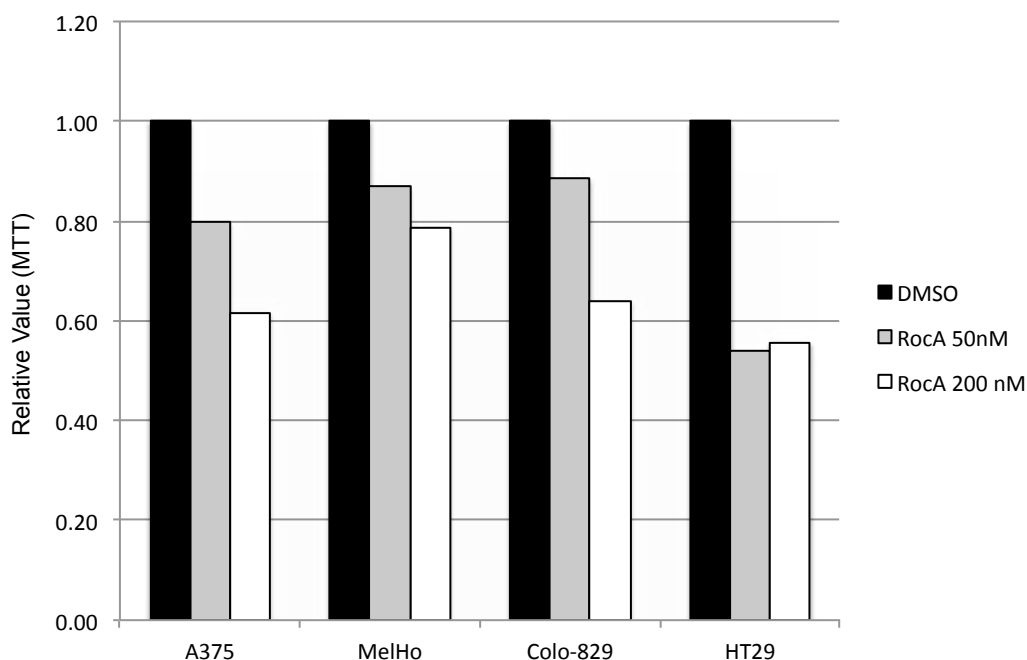


Figure S6 Rocaglamide treatment inhibit tumour cell growth in cells with BRAF mutations

Four tumour cell lines (A375, MelHo, Colo-829, HT29) with BRAF mutation were seeded in 96 well cell culture plate for 1 day and treated with Roc for 24h with two different concentrations. MTT assay was performed to obtain the amount of viable cells in the well. Shown are data from a single representative experiment where average values from 3 technical replicates were presented. The value of DMSO treated cells was taken as 1.

Supplementary figure 6

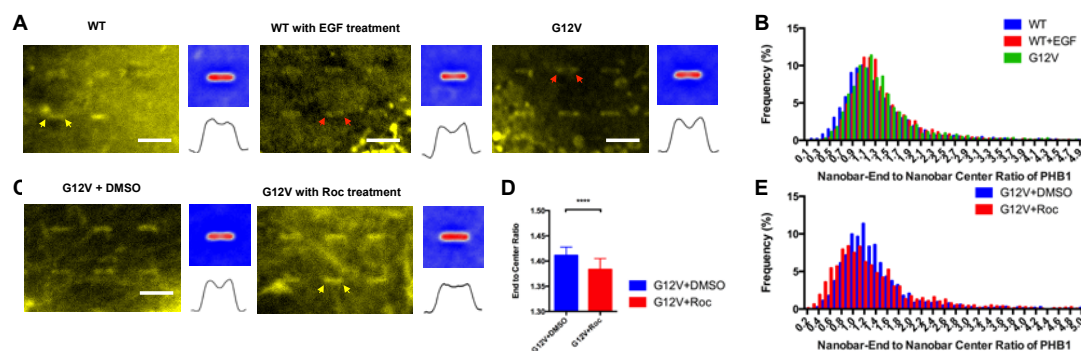


Figure S7 Rocaglamide treatment inhibit curvature response of PHB1

(A) KRAS-WT/G12V transfected U-2OS cells were cultured on nanobar arrays with/without EGF treatment and stained with Rhodamine-conjugated PHB1 binding peptide after fixation. Averaged images of WT, G12V and WT with EGF treatment on 744-1052 nanobars showed PHB1 had same distribution tendency with KRAS. Scale bar: 5 μ m. (B) Frequency distribution of end to center ratio of KRAS WT, KRAS+EGF, and KRAS G12V was shown. (C) U-2OS cells transfected with G12V were treated with rocaglamide/DMSO for 4 h before imaging. Rocaglamide affected PHB1's preference for the curved ends of the nanobars in G12V-transfected cells. Averaged images of G12V with rocaglamide or DMSO treatment on 762 or 1050 nanobars are shown. Scale bar: 5 μ m. (D) Distribution of PHB1 on each nanobar was quantified by intensity ratio of nanobar-end to nanobar-center. The distribution was quantified by averaging 744-1052 nanobars. Error bar represents SEM. Statistical significance of KRAS G12V+DMSO vs. KRAS G12V+Roc was evaluated by unpaired Kolmogorov-Smirnov test. p-value: **** p<0.0001. (E) Frequency distribution of end to center ratio of PHB1 was shown.

Supplementary table for antibody

Antibody:	Clone or Catalog Number:	Concentration	Company:
Phospho-p44/42 MAPK (Thr202/Tyr204)	9101	1/1000 in 3% BSA/PBS	Cell signaling
p44/42 MAPKinase	9192	1/1000 in 3% BSA/PBS	Cell signaling
CRAF	9422	1/1000 in 3% BSA/PBS	Cell signaling
EIF4A1	sc-377315	1/1000 in 3% BSA/PBS	Santa Cruz
Pan Ras	sc-166691	1/1000 in 3% BSA/PBS	Santa Cruz
CyclinD1	1677-1	1/1000 in 3% BSA/PBS	Epitomics
PHB1	GTX101105	1/1000 in 3% BSA/PBS	Genetex
Anti-FLAG M2 (HRP conjugated)	F3165	1/10,000 in TBS/T	Sigma
Beta-Actin (HRP conjugated)	ab49900	1/100,000 in TBS/T	Abcam
HRP conjugated anti mouse IgG	A16066	1/40,000 in TBS/T	novex
HRP conjugated anti Rabbit IgG	A16096	1/40,000 in TBS/T	novex